

DEPARTMENT OF CIVIL ENGINEERING
UNIVERSITY OF SOUTHERN CALIFORNIA

DEPENDENCE OF PSEUDO RELATIVE VELOCITY SPECTRA OF
STRONG MOTION ACCELERATION ON THE DEPTH OF SEDIMENTARY DEPOSITS

by

M.D. Trifunac and V.W. Lee

Report No. CE 79-02

A Report on the Research Conducted Under a Contract
from the U.S. Nuclear Regulatory Commission

Los Angeles, California

February, 1979

ABSTRACT

Reports on the observed damage caused by destructive earthquake ground motion and numerous instrumented studies have shown that the nature of strong shaking is influenced by the local site conditions. While the manner of characterization of these effects and the choice of their physical "basis" still represents a topic associated with many uncertainties, it has become possible, during the past several years, to improve the description of these effects empirically. This report presents some recent accomplishments in the analysis of these effects by focusing on the dependence of Pseudo Relative Velocity spectrum amplitudes on the "size" of local geologic inhomogeneities. It presents the empirical scaling functions of these spectra in terms of (a) magnitude and epicentral distance, or (b) Modified Mercalli Intensity at the site. It also considers differences between horizontal and vertical ground motions, dependence of amplitudes on depth of alluvium deposits beneath the site and the distribution of spectral amplitudes about the empirical scaling functions.

INTRODUCTION

Numerous recent studies have shown that the site conditions contribute significantly to the changes of amplitude (Trifunac and Brady, 1975; Trifunac, 1976; 1979; Trifunac and Anderson, 1977; 1978a,b; Trifunac and Lee, 1978) and of duration (Trifunac and Westermo, 1976; 1977; Westermo and Trifunac, 1978; 1979) of strong earthquake ground motion. There is little doubt now that in the linear response range, wave amplitudes with periods longer than about 0.3 sec are amplified as they propagate through "softer" geologic deposits. Amplitudes appear to be attenuated, though not significantly, for periods shorter than about 0.3 sec, thus leading to larger amplitudes of strong shaking for high frequency at igneous rock sites.

As in other wave propagation phenomena, the amplitudes of strong earthquakes waves once emitted from the source depend mainly on the variation of impedance and on the "size" of the inhomogeneities encountered along the propagation path. If the impedance jump across a discontinuity is large and if the size of the inhomogeneity is comparable to or greater than the wavelength of incident motion, major reflections and scattering will result in significant changes in the observed amplitudes of motion. Since the strong earthquake shaking of interest to earthquake engineering falls in the frequency range from about 0.1 Hz to about 20 Hz and since the seismic wave velocity near the earth's surface is in the range from about 0.1 km/sec to about 3 km/sec, it is seen that the corresponding wavelengths are from about 50 km to about 30 km. Thus, the geologic inhomogeneities of dimensions within and close

to this range will influence the observed wave amplitudes. Furthermore, since the strong shaking is typically destructive only at distances less than 50-100 km from the source (Trifunac and Brady, 1975), it is seen that the entire transmission path will contribute to the changes in wave amplitudes. It follows that the extent of "local" site conditions must be measured in terms of the wavelengths associated with the periods of motion which are most important for a particular analysis. For a tall building, a dam, or a bridge, for example, these "local" site dimensions might be of the order of 10 km. For a stiff, small building, these dimensions may be from 10 m to several hundred meters.

How the "local" site conditions change the incident wave motions depends also on the direction of wave arrival. In a realistic three-dimensional setting the wave focusing and amplification may become very complex and difficult to predict deterministically. If one knew (1) where the next earthquake will occur, and (2) if one had a realistic three-dimensional model of "local" conditions, it would be possible to compute detailed transfer functions for a site. Unfortunately, at present, neither of these two conditions can be met. The candidate sites for future earthquake loci can be speculated on only through some type of model of local seismicity. The three-dimensional geologic mapping up to the depths of say 10 km is not available for many parts of the world and when something is available, the spatial resolution and detail may not always be adequate for the purpose of deterministic computations. Even when most of the required information is available, it still will be necessary to describe the result in terms of a distribution function because: (1) earthquake sources are distributed in space

and time and their future occurrence can be described only in a probabilistic manner; and (2) the deterministic calculations of waves propagating in three dimensions through an inhomogeneous medium will, for some time, be able to provide credible results only for periods of ground motion longer than say 1 second (Anderson and Trifunac, 1977). Thus, it is seen that some type of random approach for representation of higher frequencies may be required.

At present, many investigators continue to study the effects of local conditions by employing simplified site classification in which the overall depth of near surface soil layers is typically of the order of tens of meters. From the linear wave propagation viewpoint, it can be seen that this approach is capable of portraying the effects in the high frequency range only (say, $f > 5$ Hz). For these high frequencies (short wavelengths), inhomogeneities in the top 10 km of the earth's crust lead to significant "random" scattering so that it appears optimistic to expect that deterministic calculations for the top hundred meters near the ground surface may have any significant additional impact on the overall picture of the motion there.

Significant trends in the duration of strong shaking (Westermo and Trifunac, 1978; 1979) and in the Fourier spectrum amplitudes (Trifunac and Lee, 1978) at intermediate and at long period motion require that local effects be measured on the scale of kilometers. This suggests description of local conditions in terms of the overall geologic structure there. By using the geologic site classification of Trifunac and Brady (1975), it has been possible to develop a family of empirical scaling laws for different spectral amplitudes (Trifunac and Anderson,

1977; 1978a,b) and for the duration of strong shaking (Trifunac and Westermo, 1976; 1977). While these models will remain useful for the estimation of amplitudes and of duration of strong shaking when only limited near-surface geology is known at the site, analyses show that a more refined site classification should incorporate some measure of the "size" of the local inhomogeneities (Westermo and Trifunac, 1978; 1979; Trifunac and Lee, 1978).

The aim of this report is to show that the scaling of the Pseudo Relative Velocity (PSV) spectra can be analyzed by introducing the depth of sediments beneath the site as a scaling parameter. In general, wave velocities and rigidities increase with depth. While these increases may be irregular functions of depth, significant increases in velocity and in rigidity should be experienced at the transition from sediments into sound igneous rock. Therefore, the impedance jumps and the depth of these discontinuities may then play an important role in governing the wave amplitudes and the number of consecutive reflections (duration) of strong motion between the ground surface and this "strongest" discontinuity. While the depth of sediments alone is far from sufficient to describe all important properties of the local site conditions, other analyses show that the depth as a parameter does contribute to the changes of Fourier amplitudes and of duration.

The estimates of the depths of sedimentary and alluvial deposits beneath recording stations considered in this analysis range from 0 km to about 6 km, with most sites having depth less than about 4 km. Computation of these depths and other characteristics of the data base is described elsewhere and need not be repeated here (Westermo and Trifunac, 1978).

SCALING OF PSV SPECTRA IN TERMS OF M, R, h AND v

In following the direction of the preceding analyses (Trifunac and Lee, 1978), the dependence of the spectral amplitudes of strong motion is presented here in terms of the functional form of the definition of the local magnitude scale, M, and with a "correction" function which includes the effects of geologic site conditions (h), horizontal versus vertical motions (v=0 for horizontal and v=1 for vertical), frequency dependent attenuation and the distribution of observed amplitudes with respect to the assumed model amplitudes. In contrast with the earlier model for scaling of PSV spectrum amplitudes (Trifunac and Anderson, 1977) which was based on rough site classification (s=0 for alluvium, s=2 for igneous basement rock sites, and s=1 for intermediate sites), in this paper, we introduce a more continuous dependence on the "size" of local geologic conditions in terms of h (measured in km) and representing the depth of sediments beneath the station. The scaling equation is then

$$\log_{10}[\text{PSV}(T)] = M + \log_{10}A_0(R) - b(T)M - c(T) - d(T)h - e(T)v - f(T)M^2 - g(T)R \quad (1)$$

In (1), PSV(T) is the amplitude of PSV spectra at period T and $\log_{10}A_0(R)$ represents the empirically determined function describing the overall attenuation of amplitudes with epicentral distance, R (Richter, 1958).

The scaling functions b(T) through g(T) are determined through the regression analysis at 91 periods. This analysis is performed in such a way as to minimize the possible bias in the result that may come from uneven distribution of data among magnitude, site conditions and from the abundance of data for some earthquakes. All procedures in data

preparation and selection, and the form of the regression analysis employed here are the same as in Trifunac and Lee (1978), and in Trifunac and Anderson (1977), and thus will not be repeated here.

After smoothing along $\log_{10}T$ axis, the functions $a(T)$ through $g(T)$ (Figure 1) can be described by their amplitudes at 11 periods between $T=0.04$ sec and $T=7.5$ sec (Table I). The 11 periods appear to be sufficient for most practical computations since the smoothness of $b(T)$ through $g(T)$ is such that almost any interpolation scheme will yield adequate estimates of their amplitudes at intermediate periods.

The functional form of the dependence of $\log_{10}[\text{PSV}(T)]$ on h was examined in some detail since there is no obvious physical reason why it should be linear in h . Several regression analyses have shown that only $d(T)h$ is a significant contributor to (1) with coefficients of h^2 , h^3 and higher powers of h leading to the values which were undistinguishable from zero at 95% confidence level.

If $\hat{b}(T)$ through $\hat{g}(T)$ represent the best estimates of the functions $b(T)$ through $g(T)$, the $\log_{10}[\hat{\text{PSV}}(T)]$ represents the best estimate of $\log_{10}[\text{PSV}(T)]$ at some period T . The residuals

$$\epsilon(T) = \log_{10}[\text{PSV}(T)] - \log_{10}[\hat{\text{PSV}}(T)] \quad (2)$$

where in $\log_{10}[\text{PSV}(T)]$ the PSV spectrum is computed from recorded accelerograms then describe the distribution of the observed $\text{PSV}(T)$ about the estimated $\hat{\text{PSV}}(T)$. In this work, we assume that $\epsilon(T)$ can be described by a distribution of the form (Trifunac and Anderson, 1977; 1978a)

$$p(\epsilon, T) = [1 - \exp(-\exp(\alpha(T)\epsilon(T) + \beta(T)))]^{N(T)} \quad (3)$$

where $p(\epsilon, T)$ represents the probability that $\log_{10}[\text{PSV}(T)] - \log_{10}[\hat{\text{PSV}}(T)] \leq \epsilon(T)$. From (3), it follows that $\epsilon(T) = 1/\alpha(T) [\ln(-\ln(1 - p^{1/N})) - \beta(T)]$

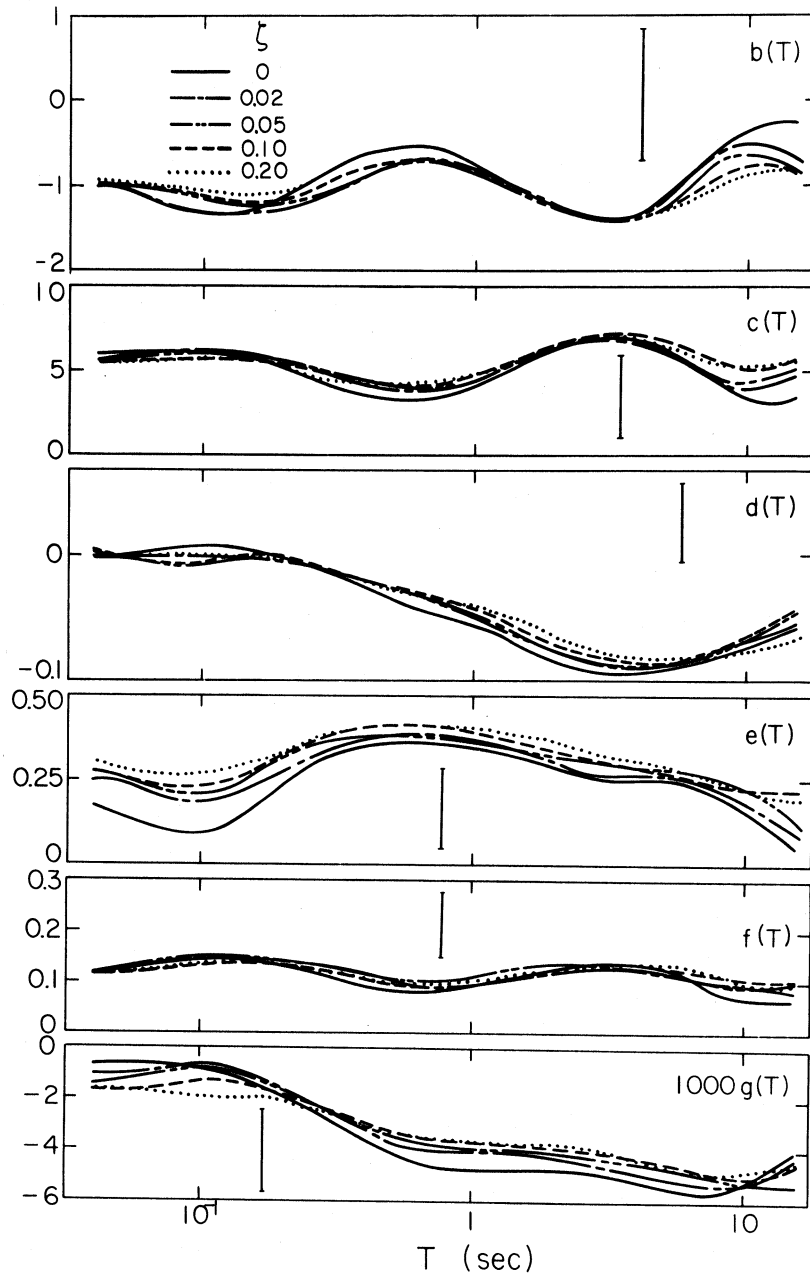


Figure 1

TABLE I

Regression Parameters for Equation (1) and $\alpha(T)$, $\beta(T)$, $N(T)$ at Eleven Selected Periods

Period, T(sec)	.040	.065	0.11	0.19	0.34	0.50	0.90	1.60	2.80	4.40	7.50
$\zeta = 0.0$											
b(T)	-1.020	-1.140	-1.320	-1.150	-0.748	-0.577	-0.717	-1.110	-1.380	-1.250	-0.600
c(T)	5.950	6.090	6.150	5.240	3.850	3.350	4.030	5.670	6.810	6.420	4.260
10*d(T)	0.011	0.023	0.046	-0.039	-0.217	-0.344	-0.524	-0.747	-0.929	-0.932	-0.806
e(T)	0.168	0.120	0.109	0.227	0.329	0.344	0.342	0.311	0.260	0.250	0.217
f(T)	0.125	0.133	0.146	0.132	0.101	0.087	0.094	0.117	0.136	0.130	0.087
1000*g(T)	-0.757	-0.795	-0.972	-1.850	-3.140	-3.970	-4.590	-4.540	-4.680	-5.150	-5.530
$\alpha(T)$	1.280	1.190	1.150	1.240	1.340	1.350	1.410	1.420	1.400	1.780	2.710
$\beta(T)$	1.000	0.988	0.977	0.985	0.992	0.995	0.912	0.760	0.491	-0.021	-0.691
N(T)	10	10	10	10	10	10	8	6	4	2	1
$\zeta = 0.02$											
b(T)	-0.978	-1.080	-1.280	-1.270	-0.980	-0.784	-0.803	-1.120	-1.410	-1.300	-0.675
c(T)	5.750	5.890	6.060	5.660	4.620	4.090	4.420	5.790	7.030	6.660	4.570
10*d(T)	0.006	-0.003	0.004	-0.035	-0.135	-0.246	-0.457	-0.680	-0.846	-0.875	-0.783
e(T)	0.254	0.213	0.191	0.271	0.353	0.367	0.364	0.326	0.275	0.266	0.229
f(T)	0.125	0.132	0.148	0.148	0.124	0.106	0.101	0.119	0.140	0.134	0.092
1000*g(T)	-1.090	-0.868	-0.709	-1.600	-2.950	-3.670	-4.100	-4.160	-4.410	-4.900	-5.460
$\alpha(T)$	1.630	1.490	1.380	1.410	1.490	1.490	1.530	1.510	1.440	1.800	2.720
$\beta(T)$	1.010	0.997	0.990	0.997	1.000	1.000	0.910	0.742	0.473	-0.300	-0.683
N(T)	10	10	10	10	10	10	8	6	4	2	1
$\zeta = 0.05$											
b(T)	-0.928	-1.010	-1.180	-1.200	-0.945	-0.771	-0.821	-1.130	-1.400	-1.320	-0.761
c(T)	5.260	5.710	5.810	5.490	4.590	4.120	4.550	5.870	7.050	6.800	4.940
10*d(T)	-0.009	-0.040	-0.042	-0.025	-0.101	-0.220	-0.421	-0.636	-0.812	-0.855	-0.781
e(T)	0.270	0.240	0.229	0.294	0.365	0.381	0.381	0.351	0.304	0.292	0.254
f(T)	0.121	0.127	0.141	0.143	0.122	0.105	0.103	0.120	0.138	0.134	0.097
1000*g(T)	-1.220	-1.050	-0.835	-1.560	-2.790	-3.420	-3.850	-3.990	-4.130	-4.350	-4.870
$\alpha(T)$	1.670	1.560	1.470	1.490	1.560	1.560	1.600	1.570	1.480	1.820	2.710
$\beta(T)$	1.010	1.000	0.995	1.000	1.000	1.000	0.908	0.740	0.471	-0.039	-0.715
N(T)	10	10	10	10	10	10	8	6	4	2	1

and this result can then be employed to calculate from (1) the spectral amplitudes which have a probability p of not being exceeded.

The probability $p^*(\epsilon, T)$ that $\epsilon(T)$ will not be exceeded can be calculated at different periods T from amplitudes of $PSV(T)$ spectra computed from recorded accelerograms and from $\hat{PSV}(T)$ estimated from (1). After finding the fraction of the residuals $\epsilon(T)$ which are smaller than a chosen value, for $P^*(\epsilon, T) = 0.1, 0.2, \dots, 0.8$ and 0.9 , $\epsilon(T)$ smoothed along the $\log_{10} T$ axis then appears as in Figure 2 for five fractions of critical damping, $\zeta = 0.0, 0.02, 0.05, 0.10$ and 0.20 . The smoothed surface $p^*(\epsilon, T)$ thus represents the distribution of data ($\log_{10}[PSV(T)]$, computed from recorded accelerograms) with respect to the estimate $\log_{10}[\hat{PSV}(T)]$ in equation (1).

By means of a regression of equation (3) on the data presented in Figure 2, it is possible to compute the estimates of $\alpha(T)$, $\beta(T)$ and $N(T)$ at 91 periods between 0.04 sec and 15 sec. Figures 3 and 4 show smoothed $\alpha(T)$, $N(T)$ and $\beta(T)$. $\alpha(T)$ and $\beta(T)$ are shown for five damping values between 0.0 and 0.20. Dependence of $N(T)$ has been neglected. Figure 5 presents the largest differences in the Kolmogorov-Smirnov test and the χ^2 amplitudes plotted versus T and assuming that the model in equation (3) with coefficients $\alpha(T)$, $\beta(T)$ and $N(T)$ as in Figures 3 and 4 describe the observed distribution. The theoretical limits on the K-S and χ^2 amplitudes for 95% confidence level are also plotted in Figure 5 and show that except for high frequencies and the χ^2 test, the model in equation (3) appears to be adequate for describing $p(\epsilon, T)$ in Figure 2. Figure 6 then presents the average, $\mu(T)$, and the standard deviation, $\sigma(T)$, for $\epsilon(T)$ in Figure 2 and for five dampings, ζ .

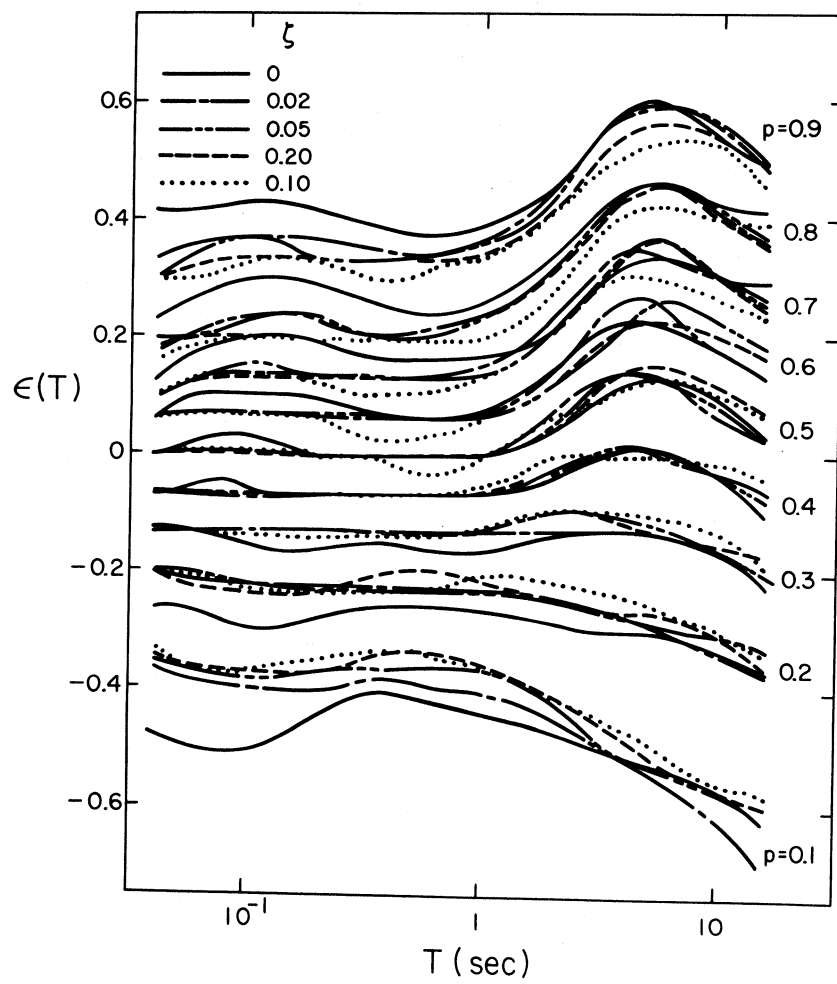


Figure 2

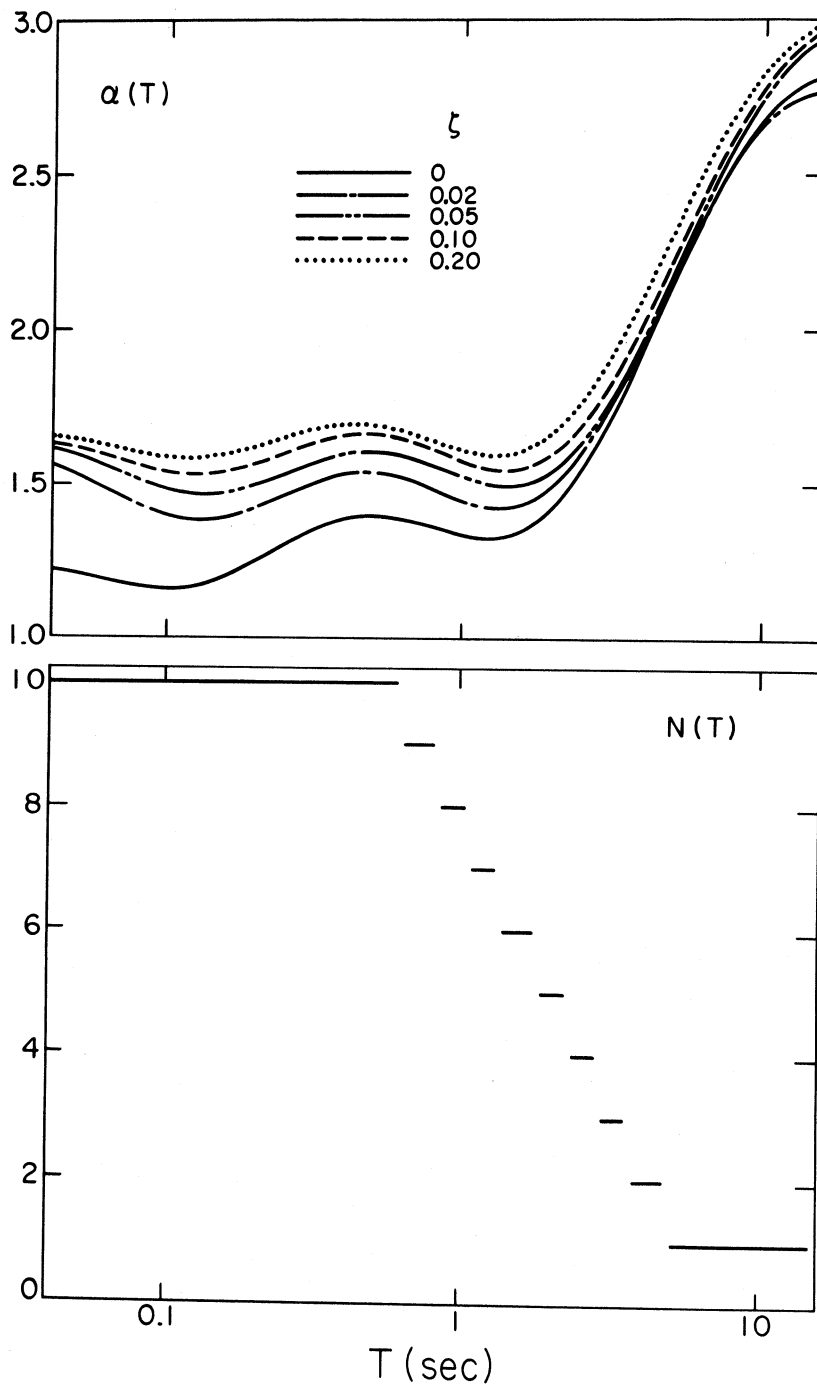


Figure 3

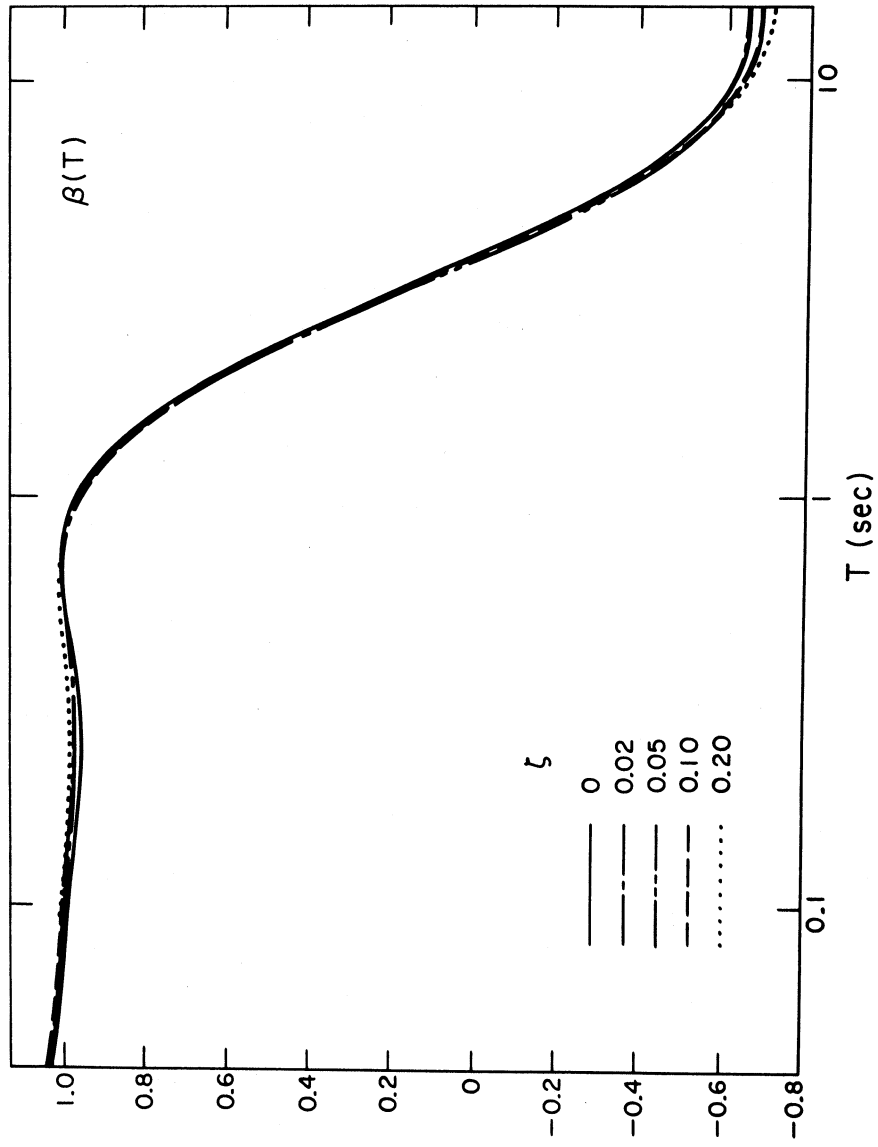


Figure 4

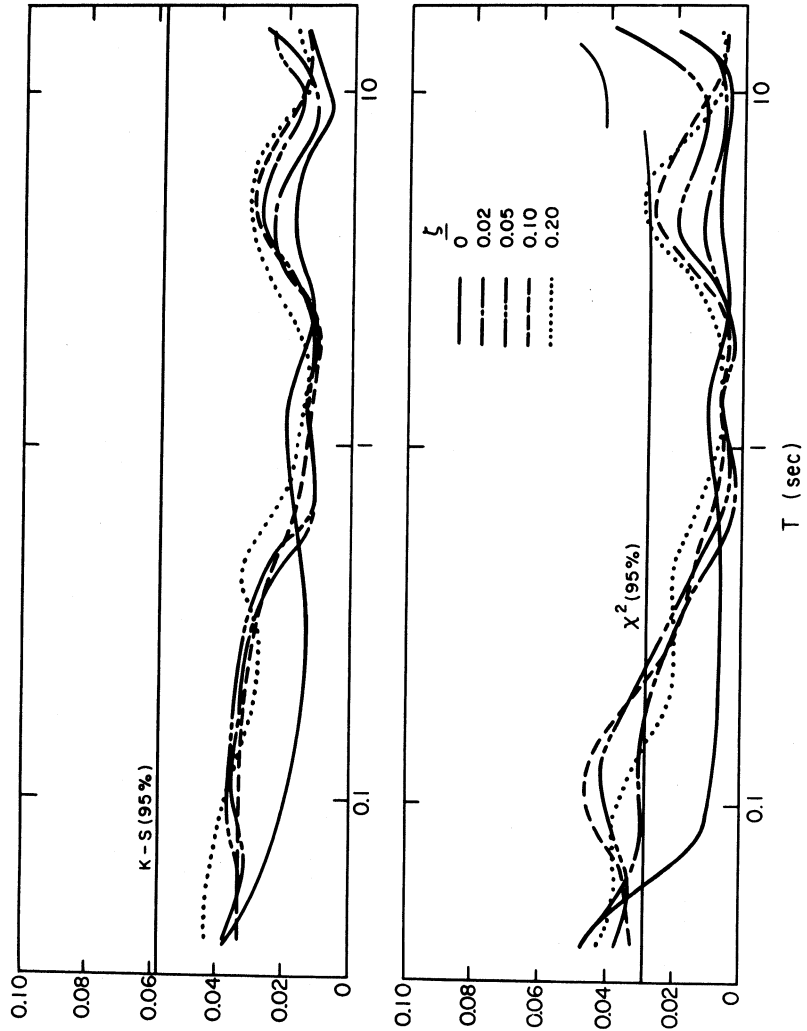


Figure 5

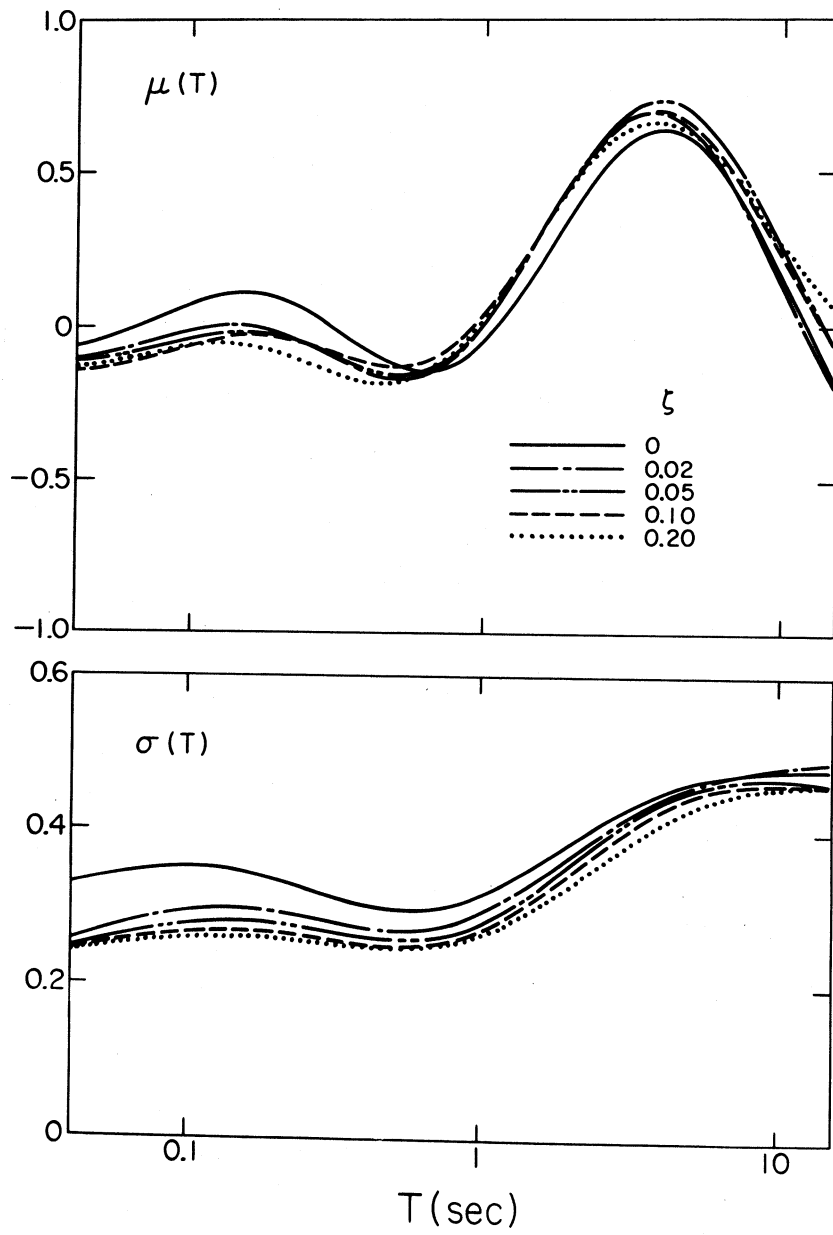


Figure 6

Table I presents the estimates of $b(T)$ through $g(T)$, $\alpha(T)$, $\beta(T)$ and $N(T)$ at eleven selected periods and for five percentages of critical damping $\zeta = 0.0, 0.02, 0.05, 0.10$ and 0.20 . Approximate significance tests (Westermo and Trifunac, 1978) of the coefficient functions $b(T)$ through $g(T)$ (vertical bars in Figure 1 correspond to the 95% confidence interval) show that all these functions are significantly different from zero in large subregions of the entire interval $T \in [0.04 \text{ sec}, 15 \text{ sec}]$. The function $d(T)$, for example, is significantly different from zero for periods longer than about 0.3 sec. Table II presents $\log_{10} A_0(R)$ which has been empirically determined for southern California (Richter, 1958).

Equation (1) applies in the interval $M_{\min} \leq M \leq M_{\max}$, where $M_{\min} = -b(T)/(2f(T))$ and $M_{\max} = (1 - b(T))/(2f(T))$. For $M \leq M_{\min}$, M is used only in the first term M in equation (1), while in the terms $b(T)M$ and $f(T)M^2$, M_{\min} is used. For $M \geq M_{\max}$, $M = M_{\max}$ is used in all terms of (1). The reasons for this are described in Trifunac (1976) and in Trifunac and Anderson (1977), and reflect the observations that the local Richter magnitude scale, which is representative of most data employed in this analysis, appears to become saturated as M grows beyond 7 to 7.5.

Figures 7 through 16 present examples of $PSV(T)$ spectra computed from equation (1) and for $M = 4.5, 5.5, 6.5$ and 7.5 , for $h = 0$ and 4 km , for $p = 0.5$ and for $\zeta = 0.0, 0.02, 0.05, 0.10$ and 0.20 . The shaded regions in these and many subsequent figures represent the range between average and average plus one standard deviation of minimum recording and digitization noise amplitudes. These noise amplitudes have been computed by digitization of a fine straight line (Trifunac, 1976) which is 2 to 3 times narrower than the 4x enlargements of typical acceleration

TABLE II
 $\log_{10}A_0(R)$ Versus Epicentral Distance R*

R(km)	$-\log_{10}A_0(R)$	R(km)	$-\log_{10}A_0(R)$	R(km)	$-\log_{10}A_0(R)$
0	1.400	70	2.805	190	3.480
5	1.500	80	2.920	200	3.530
10	1.605	85	2.958	210	3.581
15	1.716	90	2.989	220	3.631
20	1.833	95	3.020	230	3.680
25	1.955	100	3.044	240	3.729
30	2.078	110	3.089	250	3.779
35	2.199	120	3.135	260	3.828
40	2.314	130	3.182	270	3.877
45	2.421	140	3.230	280	3.926
50	2.517	150	3.279	290	3.975
55	2.603	160	3.328	300	4.024
60	2.679	170	3.378	310	4.072
65	2.746	180	3.429	320	4.119
R(km)	$-\log_{10}A_0(R)$	R(km)	$-\log_{10}A_0(R)$		
330	4.164	470	4.660		
340	4.209	480	4.685		
350	4.253	490	4.709		
360	4.295	500	4.732		
370	4.336	510	4.755		
380	4.376	520	4.776		
390	4.414	530	4.797		
400	4.451	540	4.817		
410	4.485	550	4.835		
420	4.518	560	4.853		
430	4.549	570	4.869		
440	4.579	580	4.885		
450	4.607	590	4.900		
460	4.634				

* Only the first two digits may be assumed to be significant.

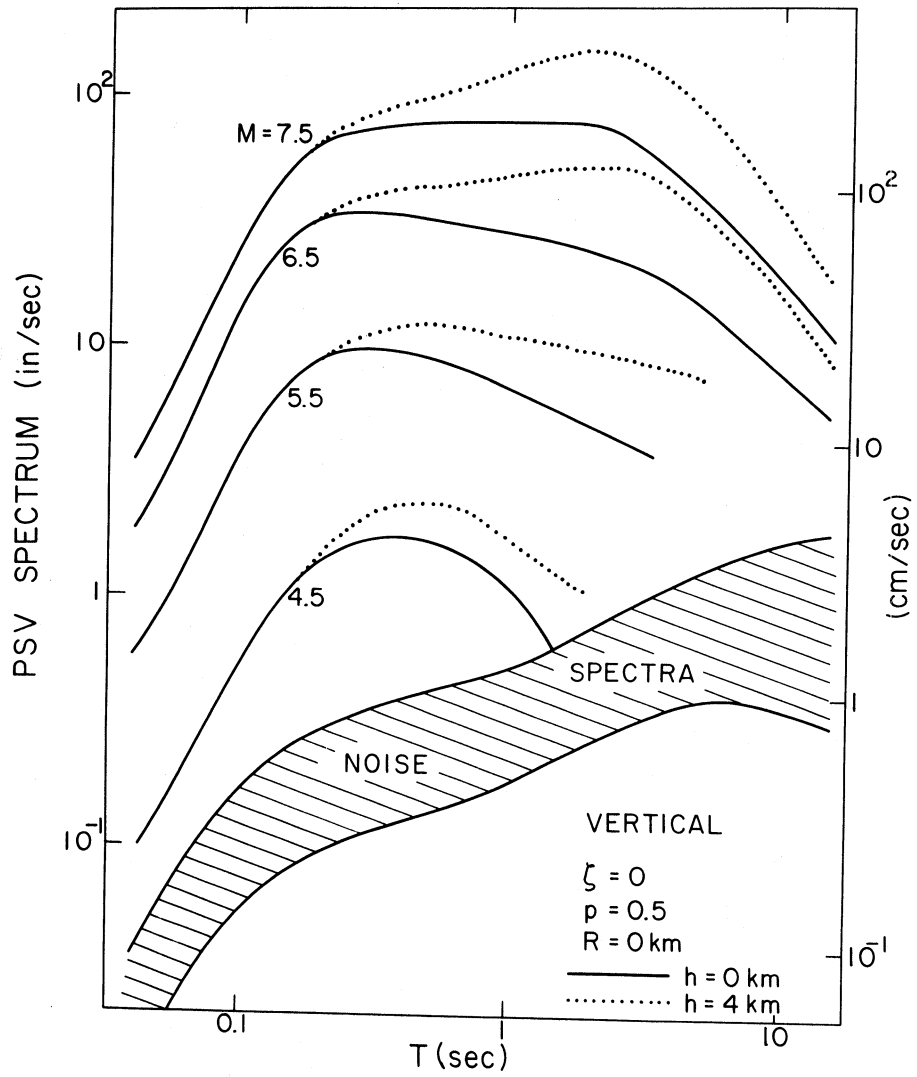


Figure 7

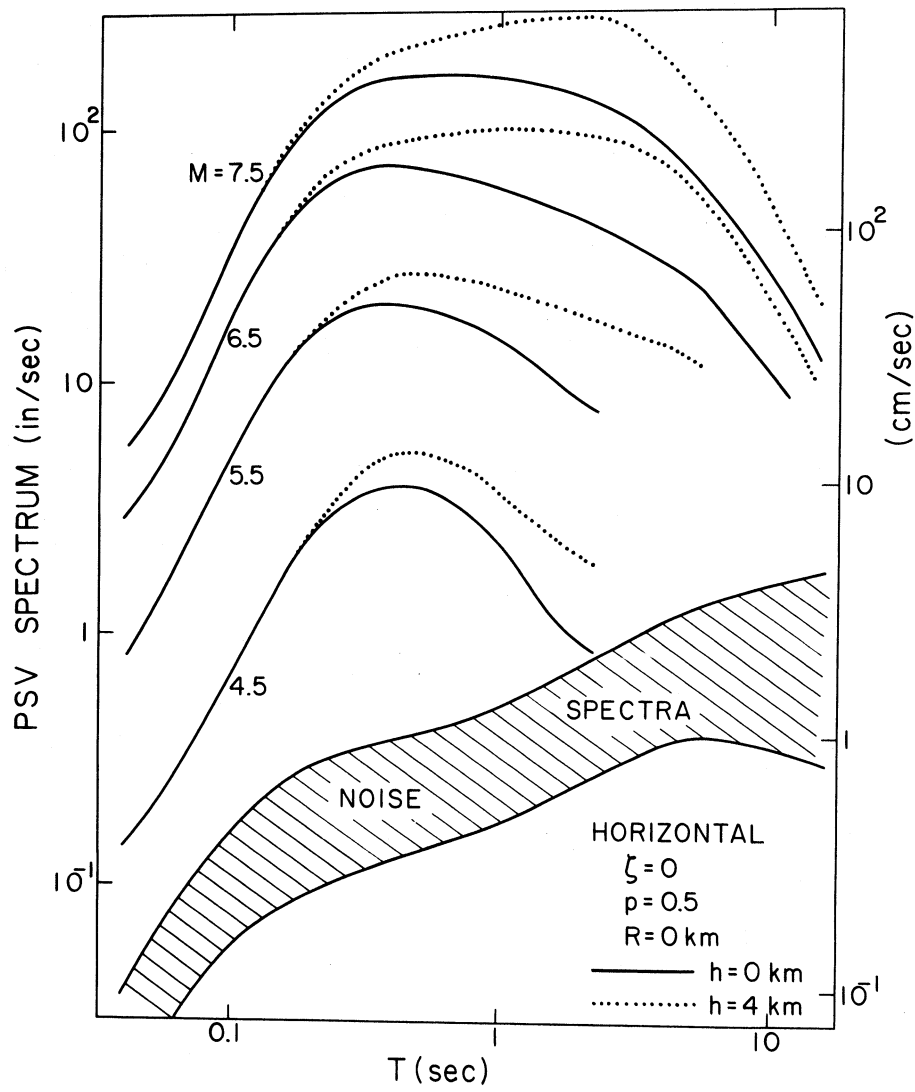


Figure 8

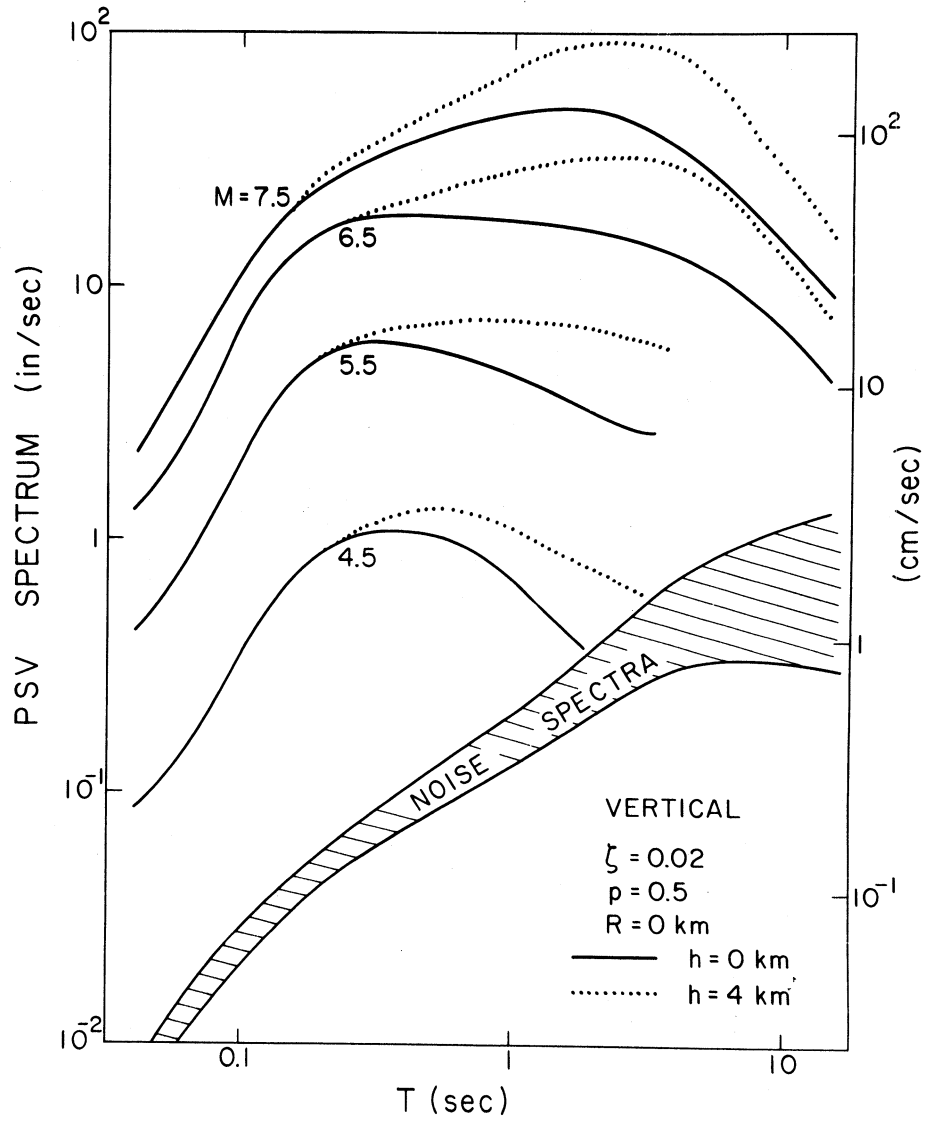


Figure 9

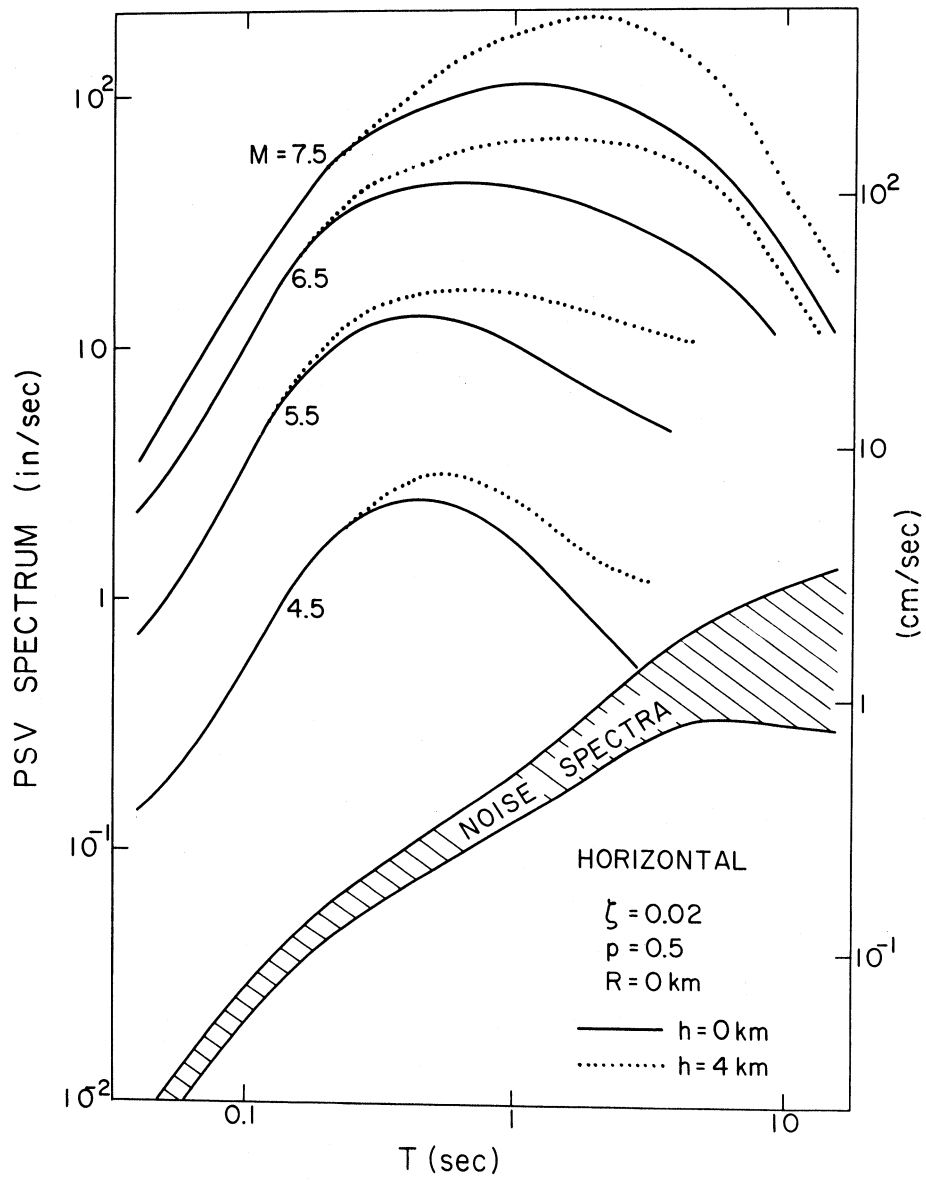


Figure 10

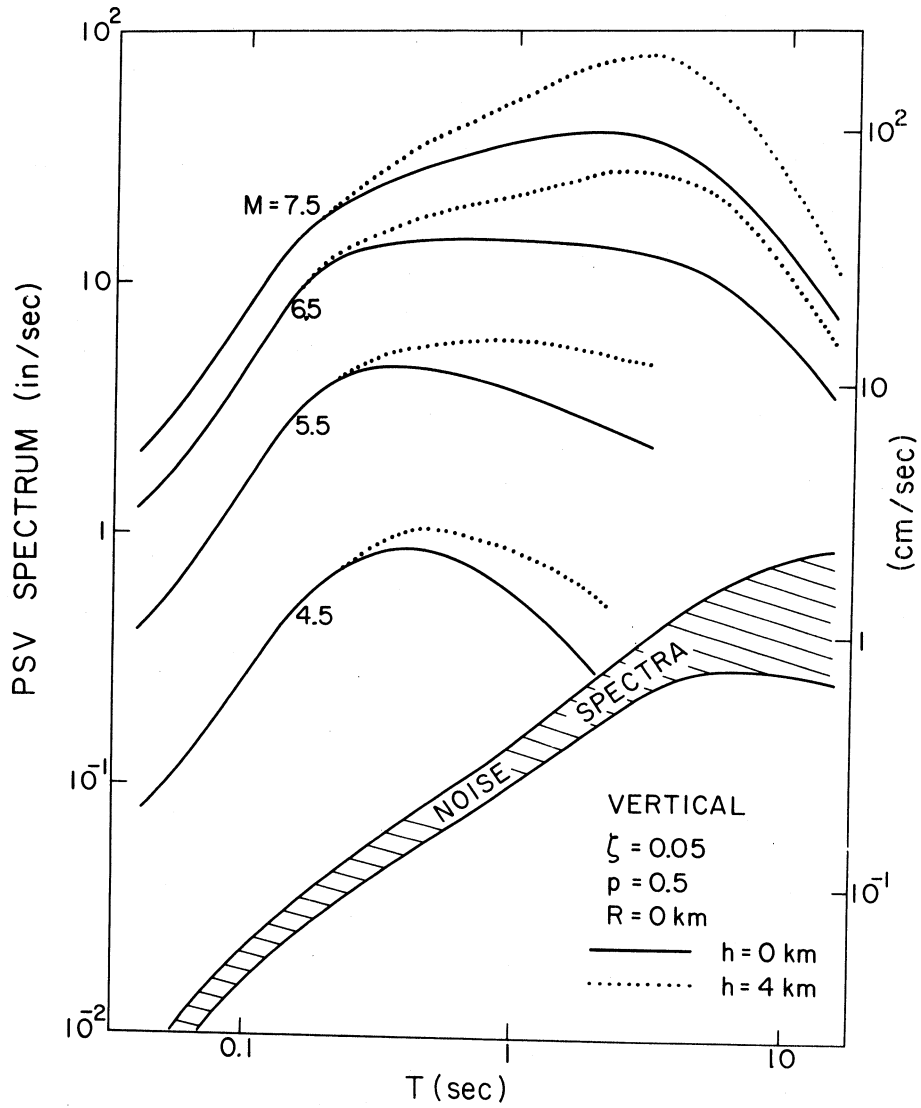


Figure 11

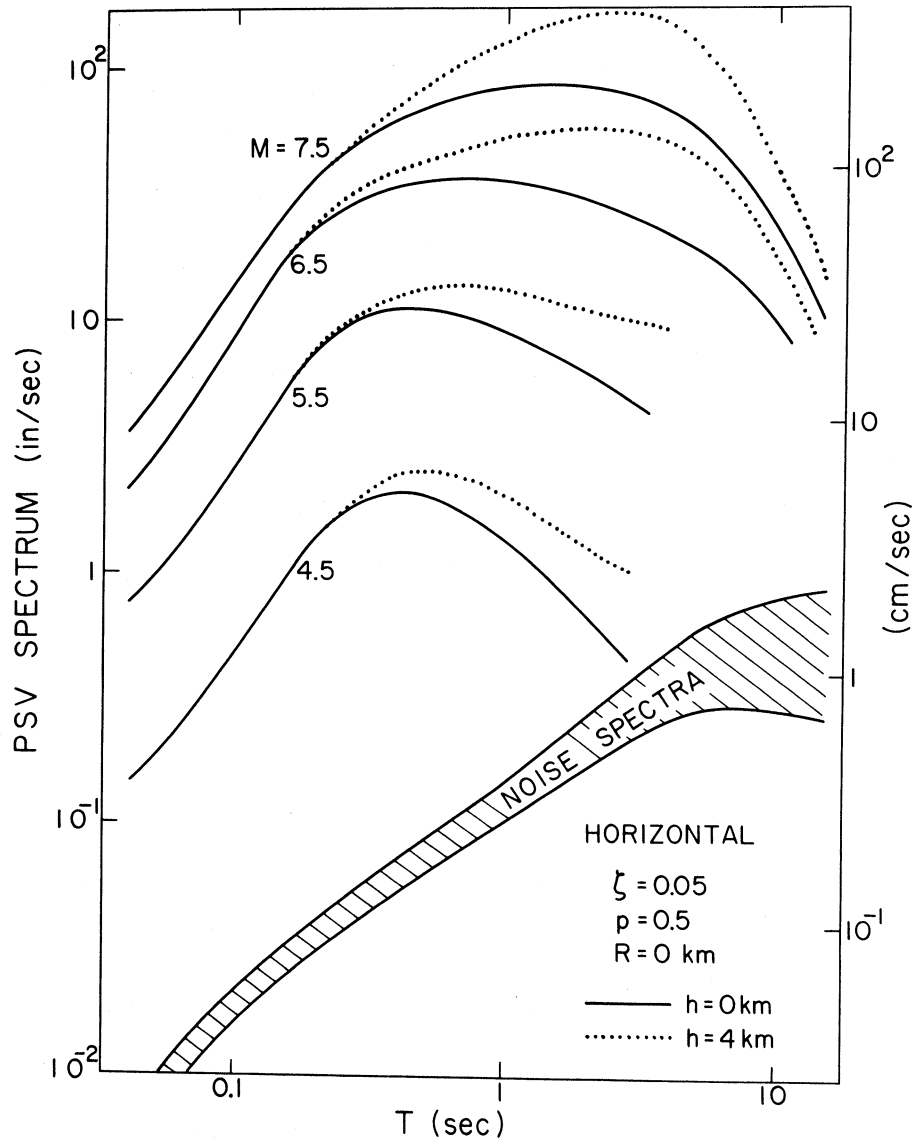


Figure 12

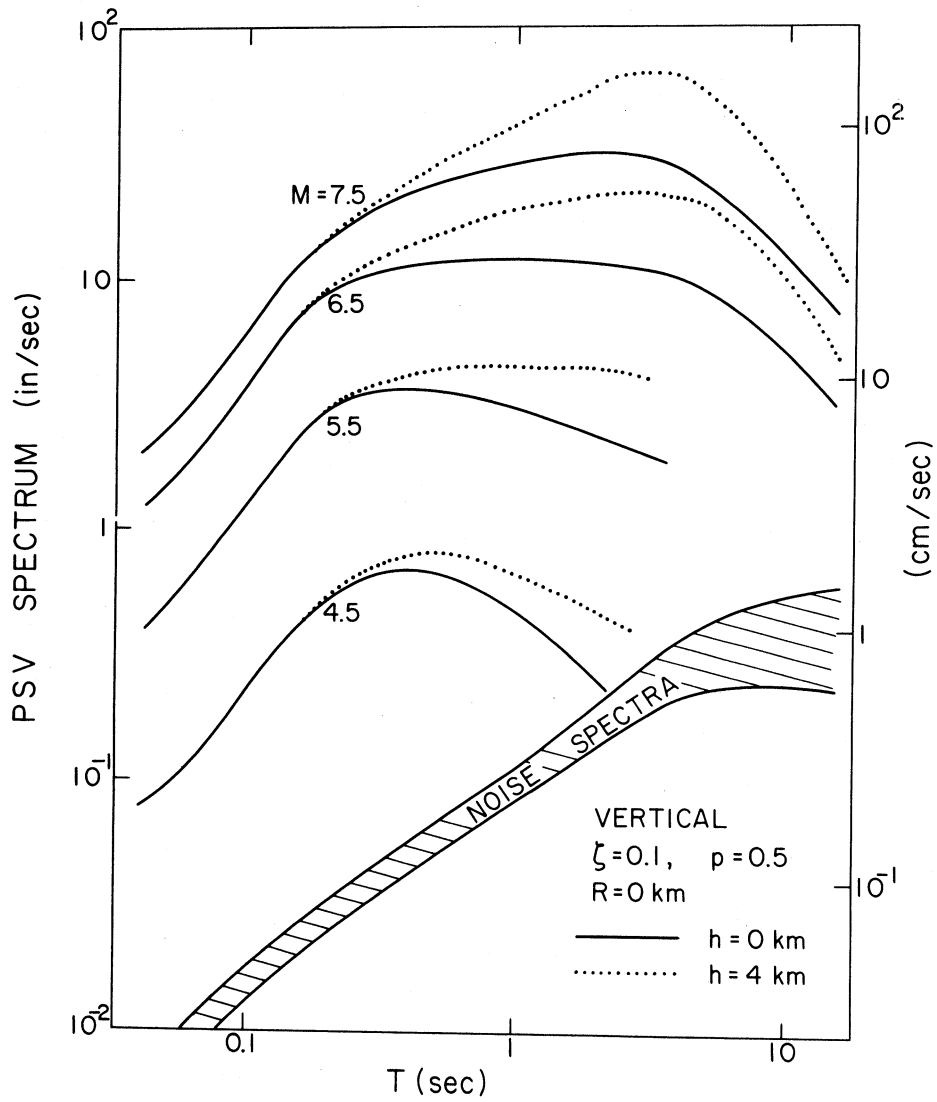


Figure 13

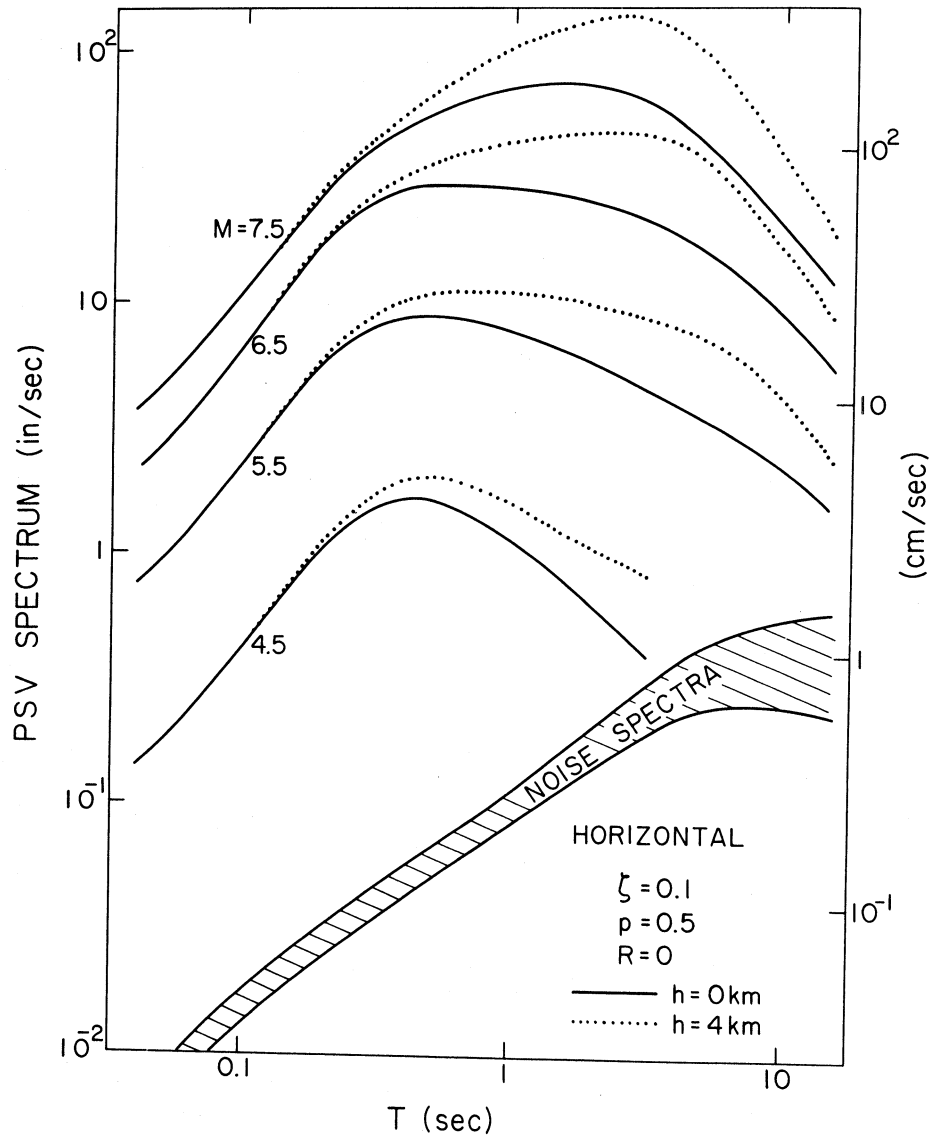


Figure 14

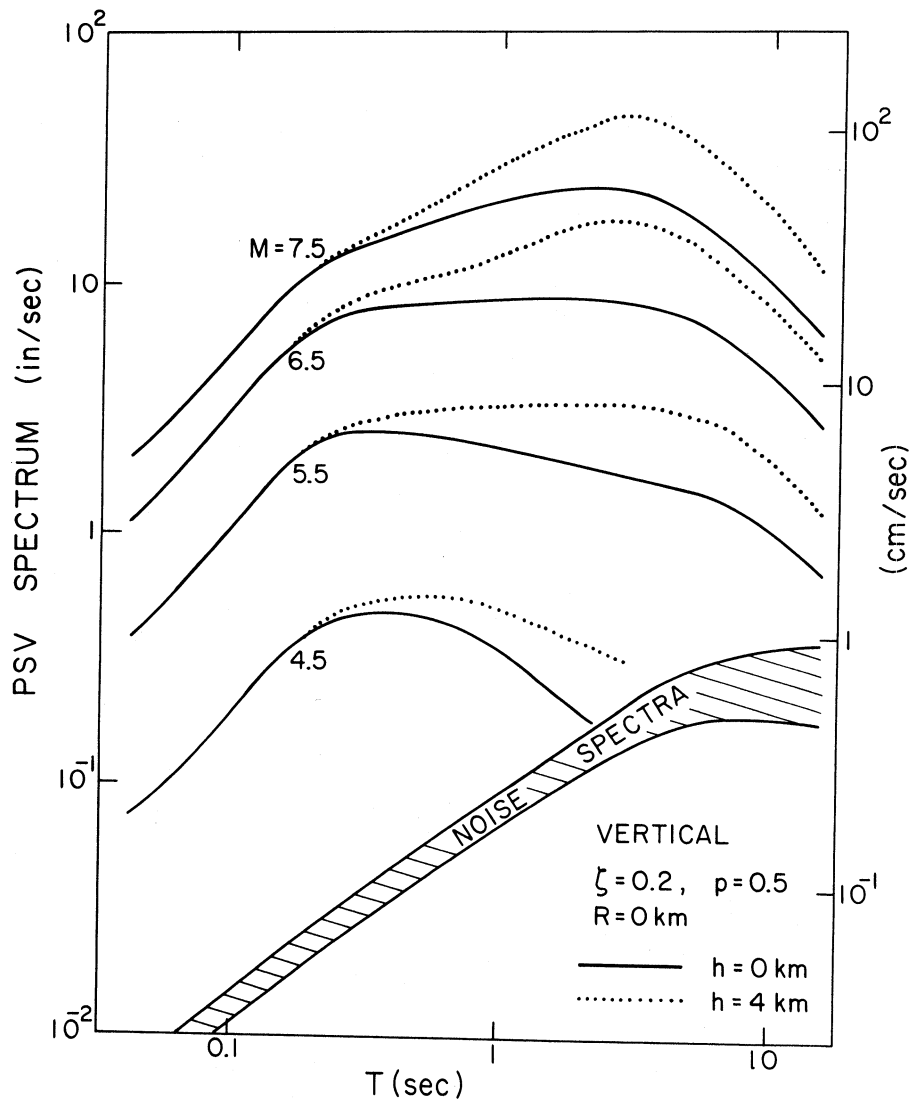


Figure 15

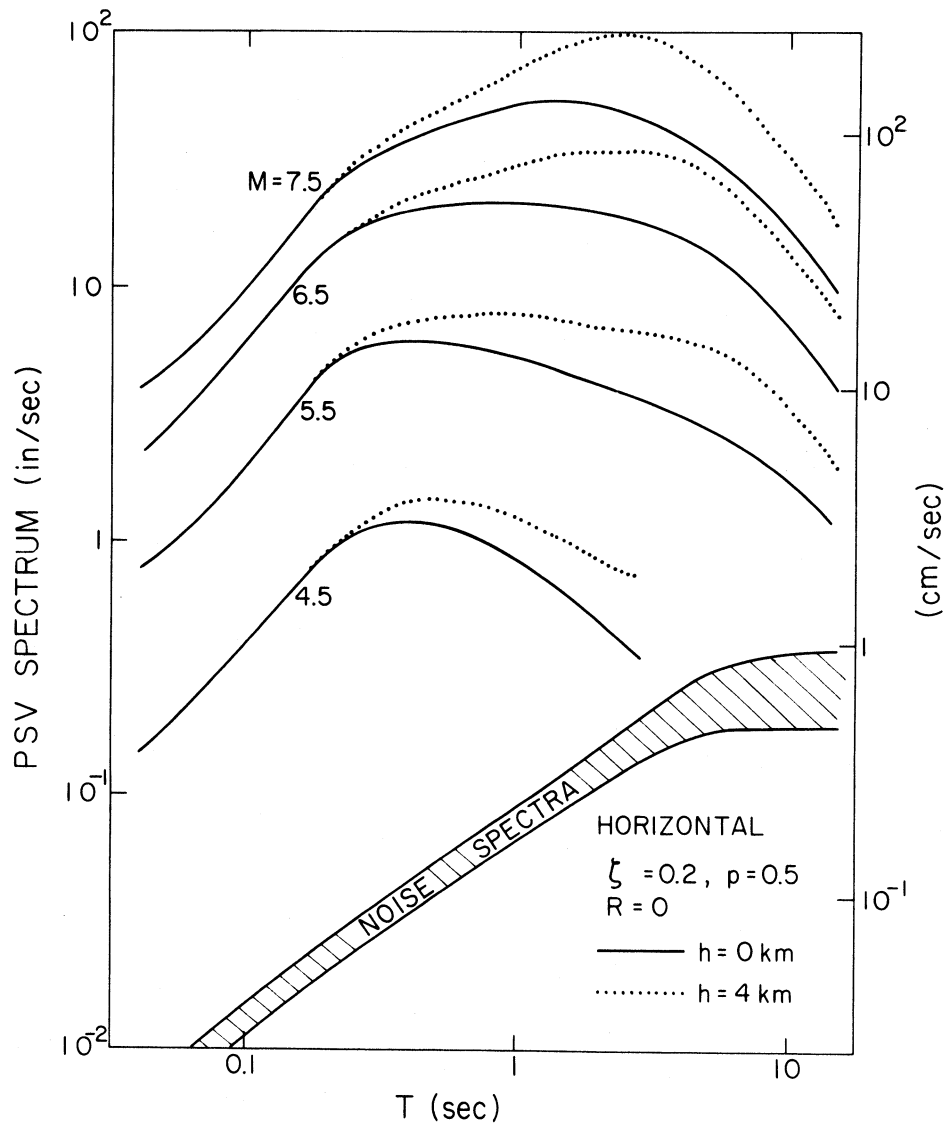


Figure 16

traces. Comparison of these noise amplitudes with the results of recent studies presented by Trifunac and Lee (1979) shows that for high frequencies ($f > 5$ Hz) spectrum amplitudes resulting from hand-digitization noise are slightly larger or comparable to the noise amplitudes resulting from well-controlled automatic digitization. At long periods, the noise amplitudes shown in figures 7 through 16 are 2 to 3 times smaller than the estimates of noise amplitudes presented by Trifunac and Lee (1979). While it appears now that the most reliable estimates of digitization and processing noise are those presented by Trifunac and Lee (1979), in all previous calculations we used the wave amplitudes as presented in Trifunac (1976). For consistency with all earlier analyses and without any significant effects on the results which are presented here, we employ the same noise amplitudes in this work.

The trends of computed PSV(T) spectrum amplitudes in Figures 7 through 16 are in many ways similar to those discussed by Trifunac and Anderson (1978a). The rate of growth of amplitudes with M clearly decreases as M approaches $M = 7.5$. The effect of local geologic conditions is important for intermediate and long periods and small for high frequencies. This is illustrated by full and dotted lines in Figures 7 through 16 which represent spectra for $h = 0$ and $h = 4$ km. The vertical spectrum amplitudes are nearly as large as the horizontal amplitudes for high frequencies.

Figures 17 through 21 illustrate the effects of epicentral distance R and damping ζ , on the changes of spectral amplitudes for $p = 0.5$, $M = 6.5$, $h = 2$ and for horizontal (full lines) and vertical (dotted lines)

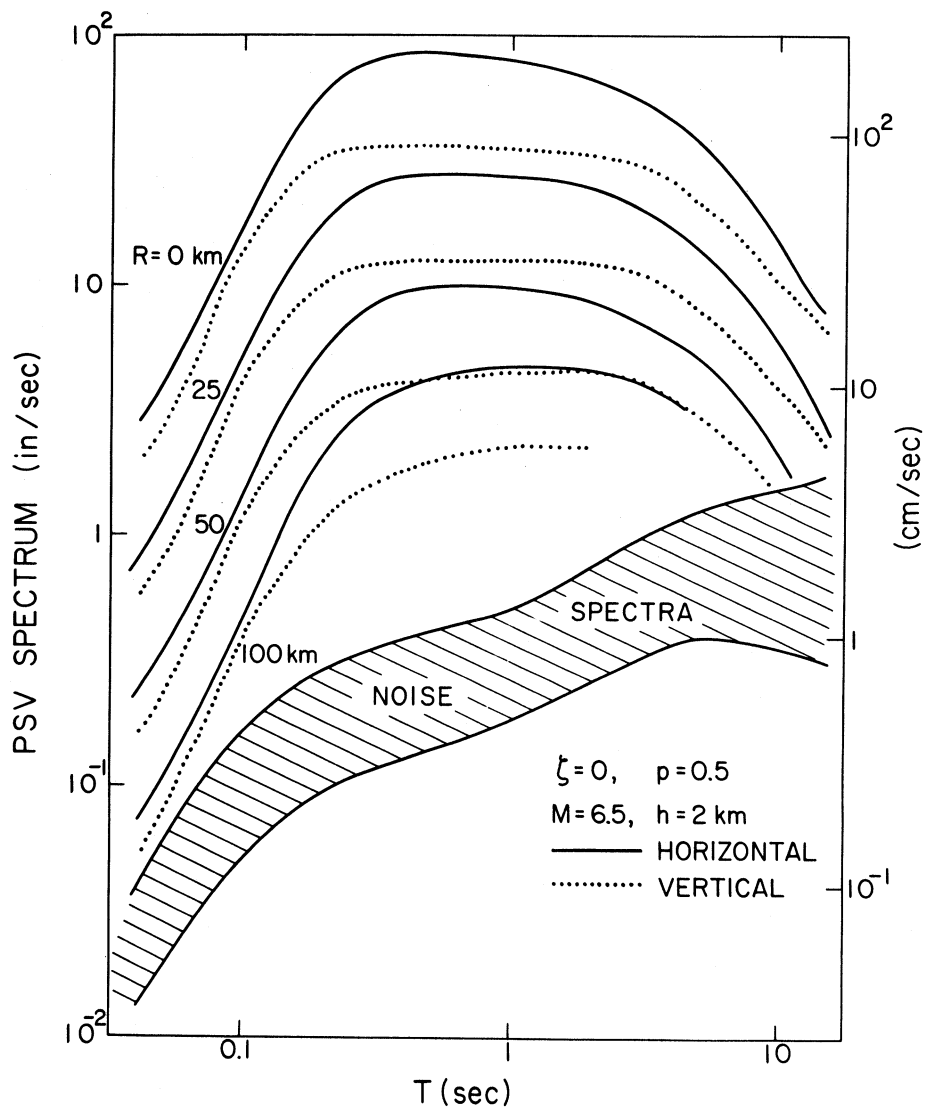


Figure 17

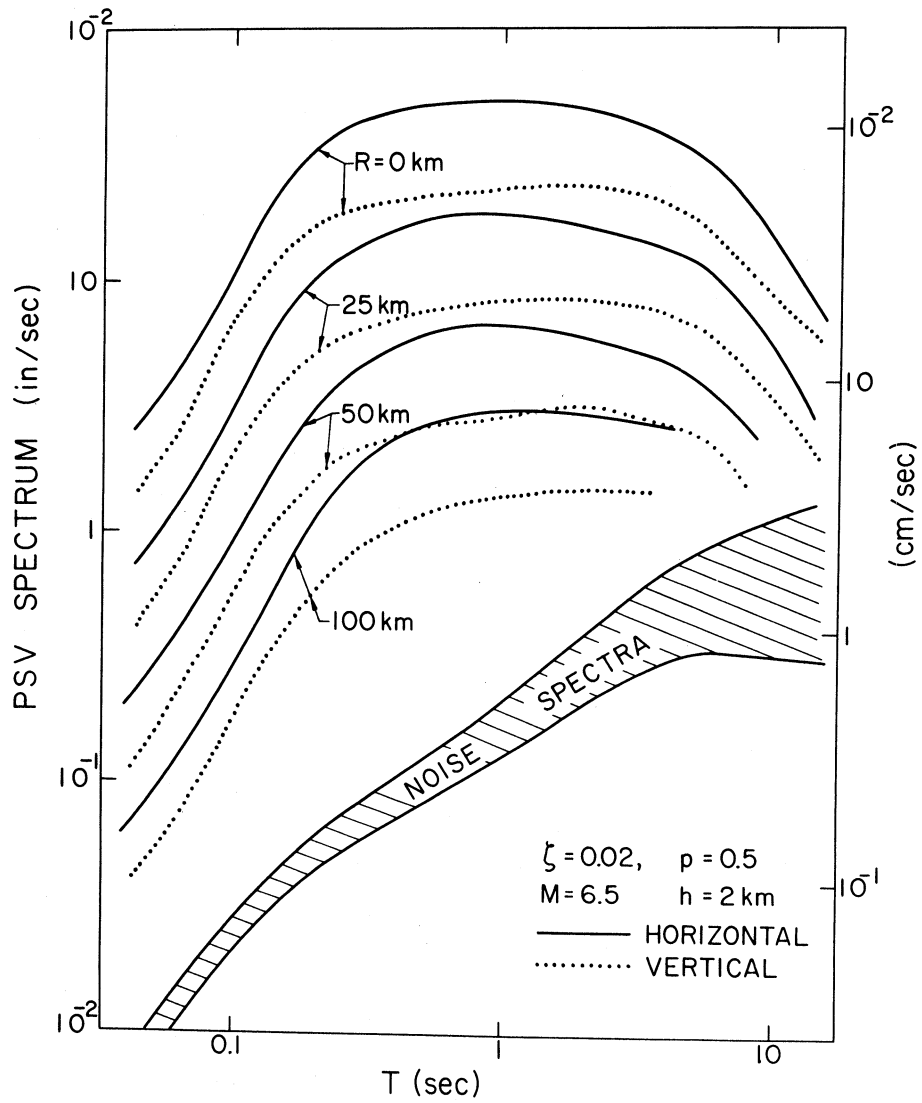


Figure 18

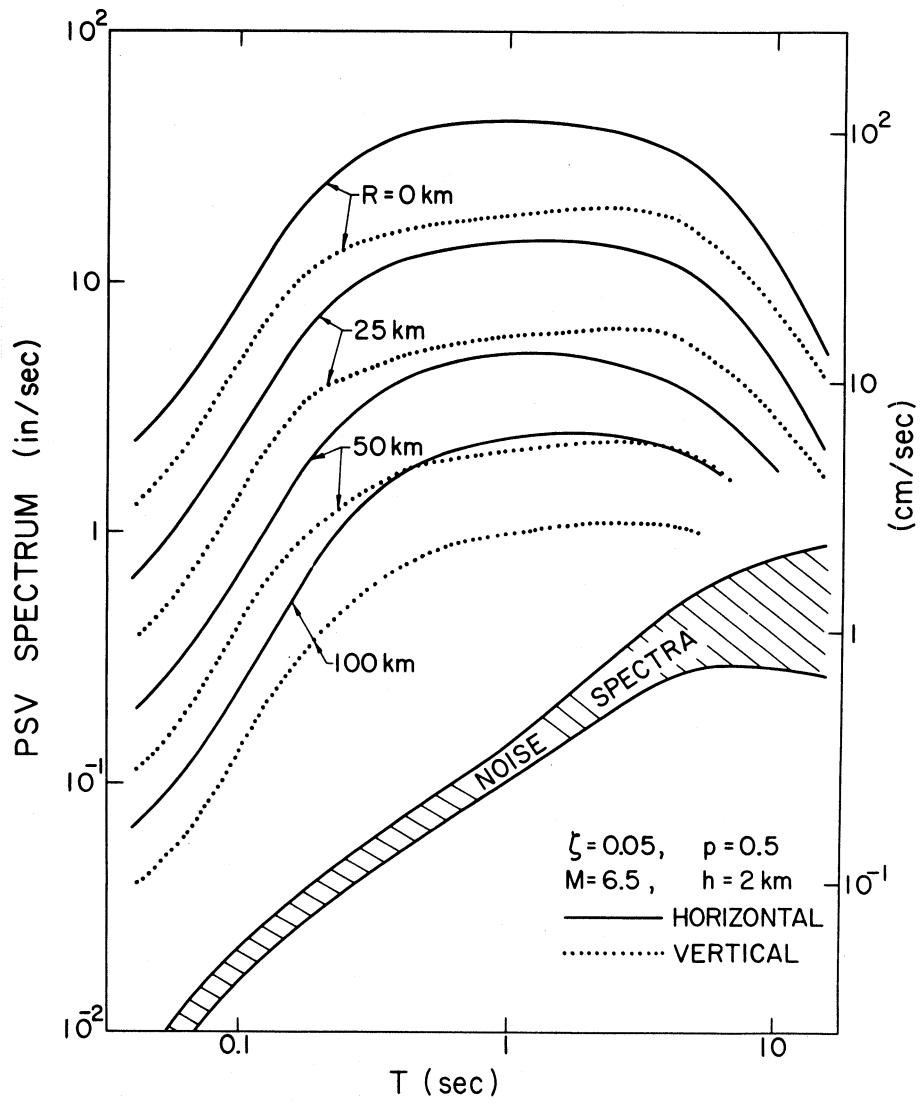


Figure 19

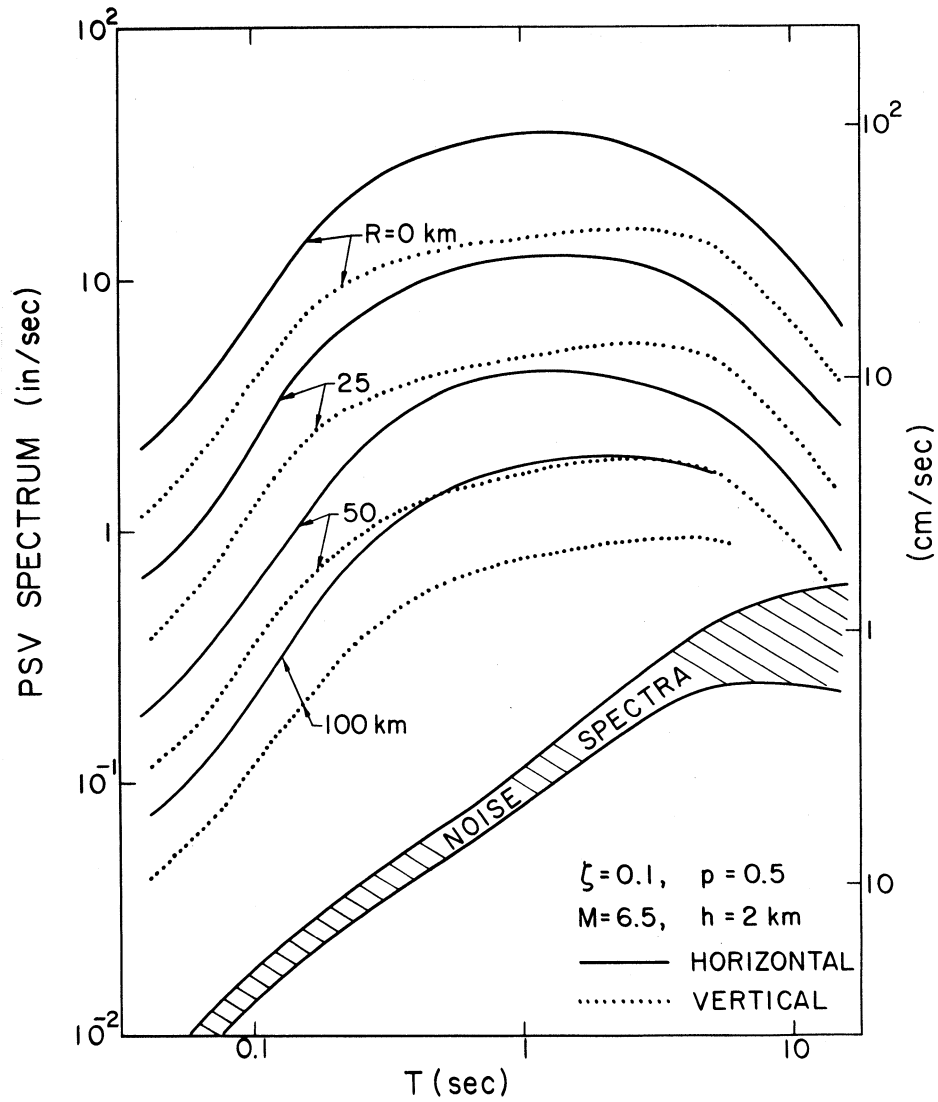


Figure 20

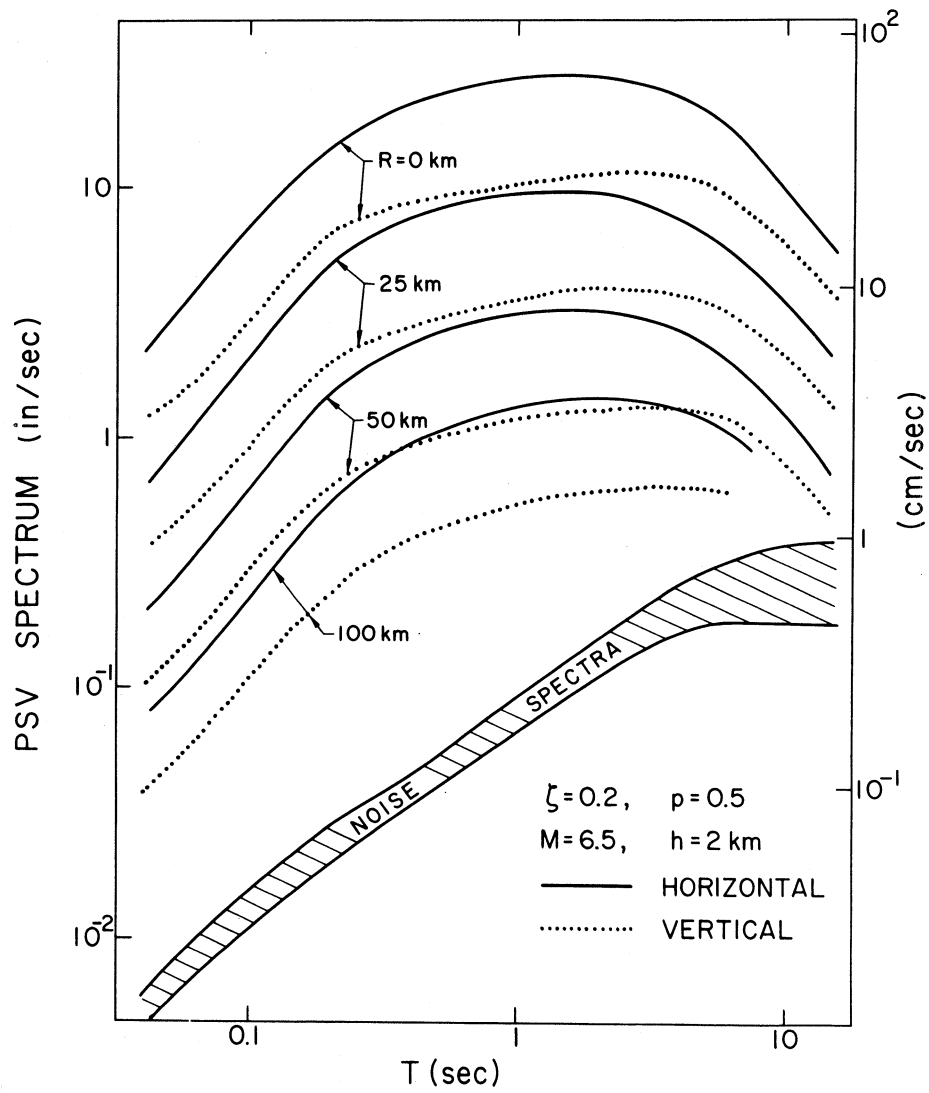


Figure 21

motions. It is seen that for small ζ vertical and horizontal spectrum amplitudes are nearly the same. With increasing damping the high frequency spectrum amplitudes of vertical motions become progressively smaller and for $\zeta = 0.20$ the shapes of horizontal and vertical spectra become similar and not too dependent on epicentral distance R .

Figures 22, 23 and 24 compare the amplitudes of PSV spectra computed from acceleration recorded during the Imperial Valley, California earthquake of 1940, in El Centro, with spectrum amplitudes from equation (1) for $p = 0.1$ and 0.9 , $M = 6.4$, $h = 19500$ ft, $R = 15$ km, $\zeta = 0.0$, 0.02 , 0.05 , 0.10 and 0.20 , and for vertical and two horizontal components. The agreement between computed and observed amplitudes is fair for vertical motions and good for horizontal motions.

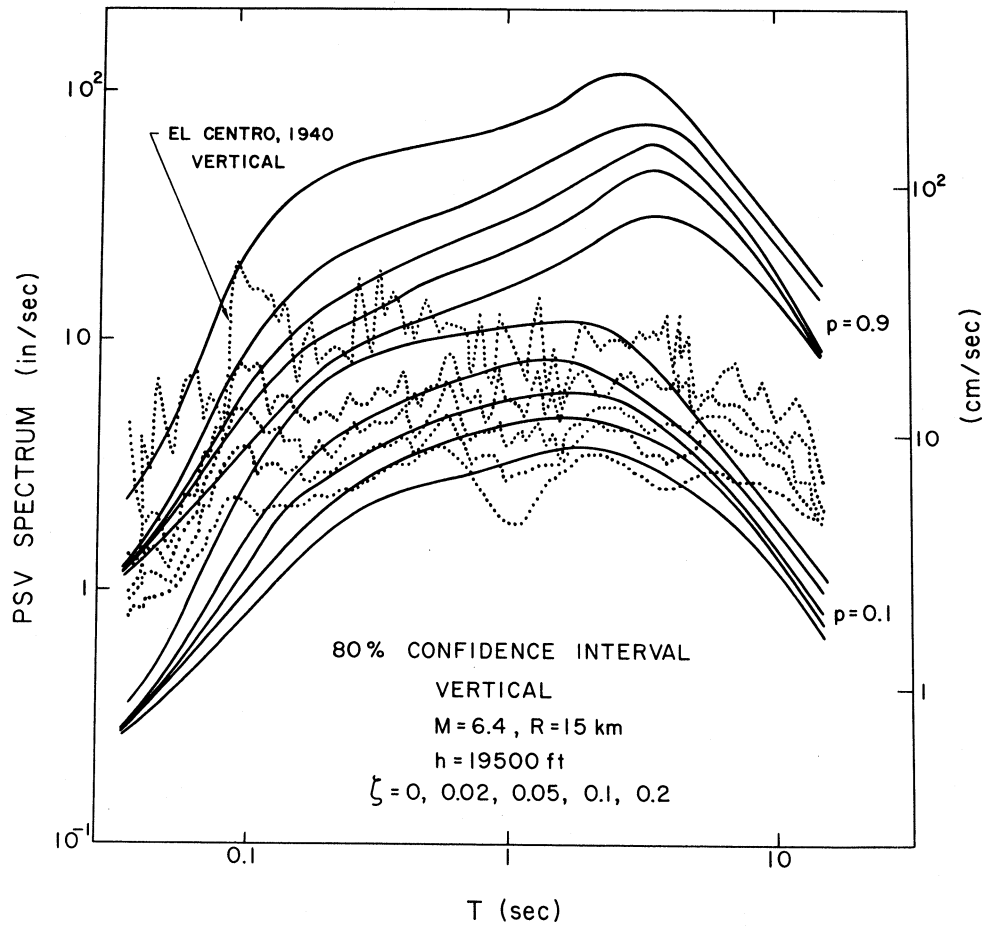


Figure 22

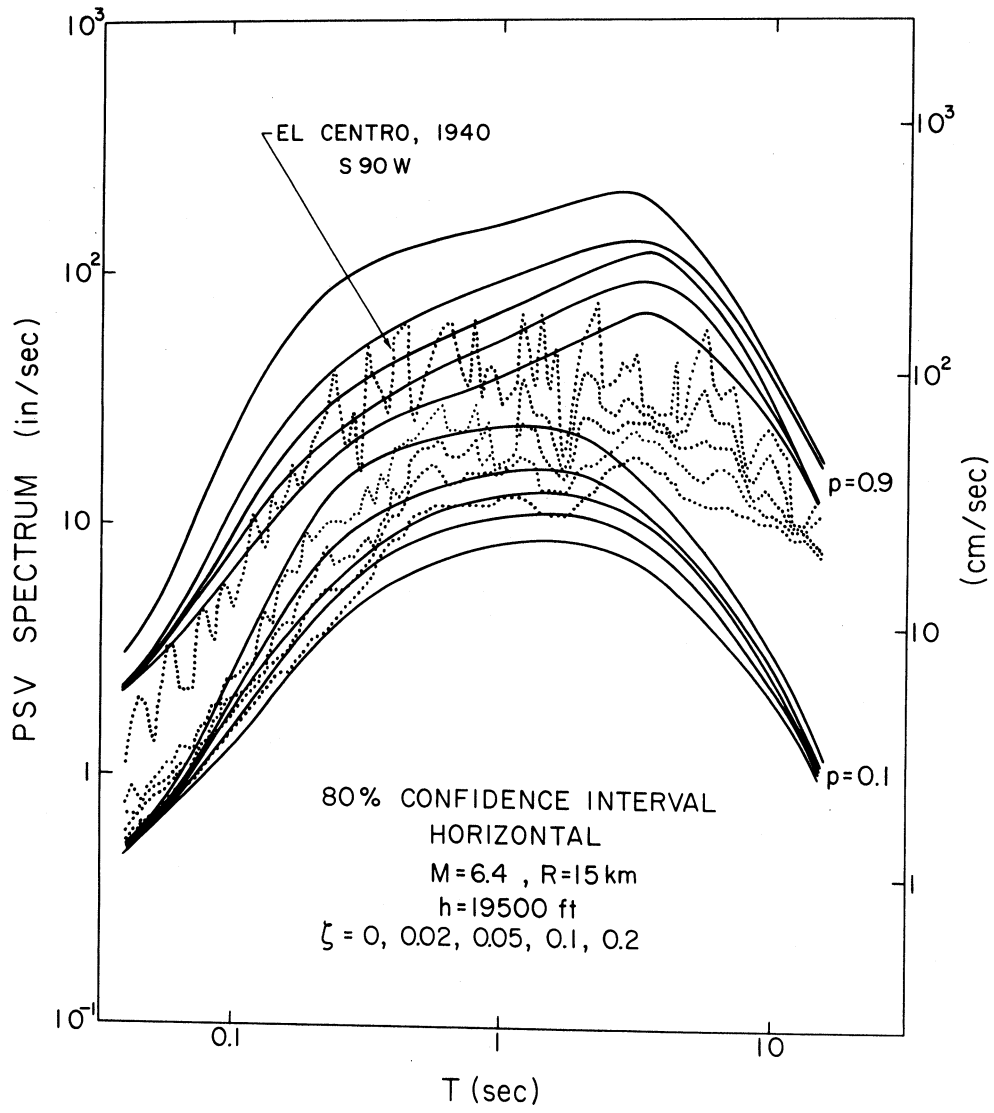


Figure 23

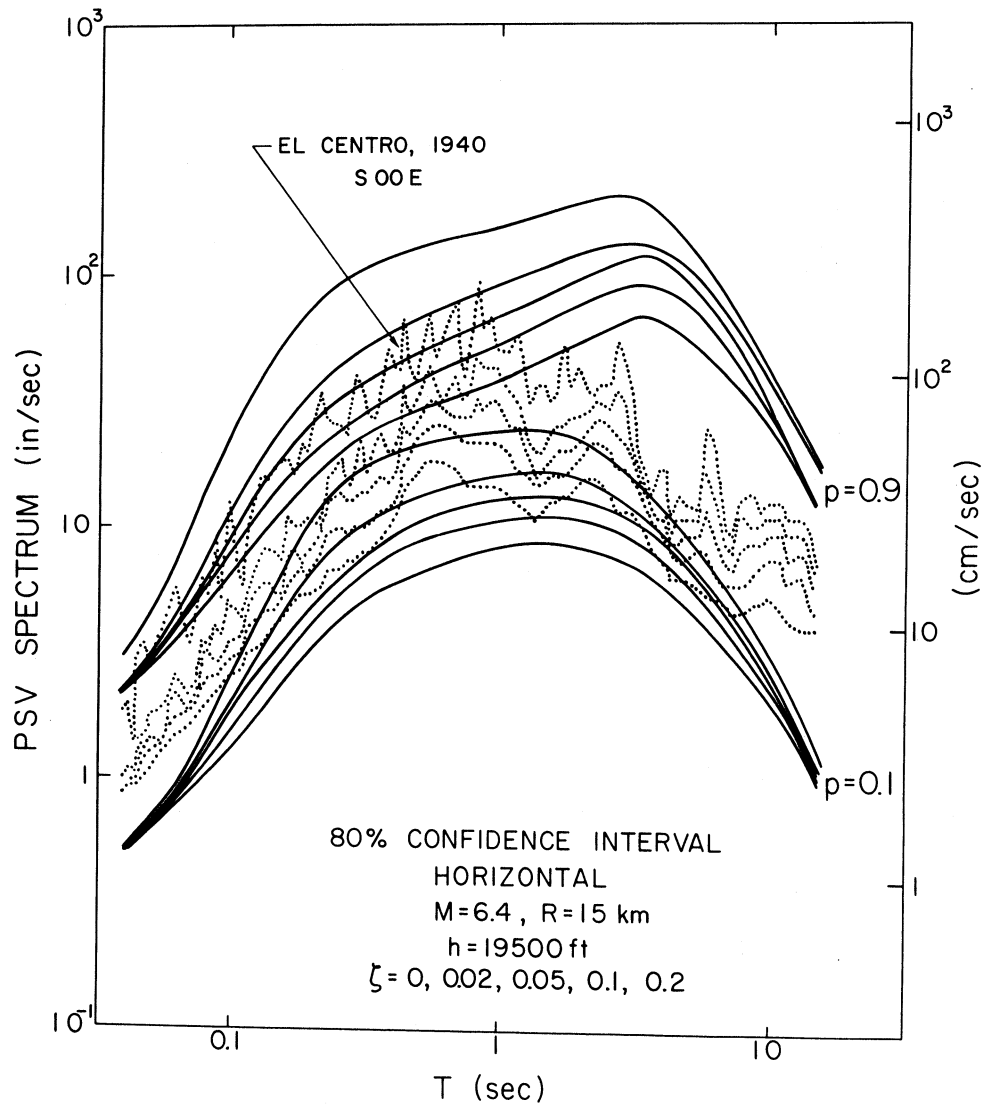


Figure 24

SCALING OF PSV SPECTRA IN TERMS OF MMI, h AND v

Following our previous work (Trifunac, 1979; Trifunac and Lee, 1978), we write

$$\log_{10}[\text{PSV}(T)] = b(T)I_{\text{MM}} + c(T) + d(T)h + e(T)v \quad (4)$$

where I_{MM} represents a numerical value (1,2,3,...,11 and 12) assigned to the corresponding level on the Modified Mercalli Intensity (MMI) at the site (I,II,..., XI and XII) (Trifunac, 1979), and h and v have the same meaning as in (1). The explicit dependence of $\text{PSV}(T)$ on epicentral distance is omitted here. Such dependence would decrease the uncertainties associated with the estimation of $\text{PSV}(T)$ in (4), but would render the expression applicable only to those regions which have similar intensity attenuation with distance as southern California, the source of most records in the present data base. Though a particular intensity of shaking can be assigned for a small nearby earthquake as for a distant large earthquake, formally equation (4) depends only on the MMI at the site and thus is more general. A recent study (Anderson, 1979) has confirmed the usefulness of this approach by showing that the end result in earthquake risk mapping based on equation (4) leads to equal or smaller uncertainties than the scaling based on equation (1) which includes explicit dependence on R .

The estimates of $b(T)$ through $e(T)$, denoted by $\hat{b}(T)$ through $\hat{e}(T)$, have been computed for the regression analysis at 91 periods between 0.04 sec and 15 sec, and smoothed along $\log_{10}T$ axis (Figure 25). Table III presents these amplitudes at eleven selected periods. Figure 26 presents the residuals $\varepsilon(T)$ as defined in equation (2) by the difference between $\log_{10}\text{PSV}(T)$ and $\log_{10}\hat{\text{PSV}}(T)$ for $\zeta = 0.0, 0.02, 0.05, 0.10$ and 0.20 .

TABLE III

Regression Parameters for Equation (4) and $\alpha(T)$, $\beta(T)$, $N(T)$ at Eleven Selected Periods

Period, T(sec)	.040	.065	0.11	0.19	0.34	0.505	0.90	1.60	2.80	4.40	7.50
$\zeta = 0.0$											
b(T)	0.349	0.332	0.300	0.276	0.266	0.267	0.291	0.325	0.328	0.292	0.235
c(T)	-2.730	-2.355	-1.605	-1.061	-0.833	-0.809	-1.006	-1.380	-1.560	-1.421	-1.240
$10^*d(T)$	-0.253	-0.276	-0.283	-0.092	0.149	0.287	0.523	0.801	1.054	1.097	0.908
e(T)	-0.134	-0.099	-0.109	-0.233	-0.329	-0.347	-0.346	-0.286	-0.208	-0.212	-0.234
$\alpha(T)$	1.940	1.808	1.751	2.012	2.393	2.506	3.634	3.196	2.666	2.500	2.636
$\beta(T)$	0.230	0.211	0.184	0.175	0.176	0.181	-0.457	-0.502	-0.531	-0.533	-0.492
N(T)	2	2	2	2	2	2	1	1	1	1	1
$\zeta = 0.02$											
b(T)	0.310	0.307	0.298	0.286	0.279	0.282	0.307	0.341	0.348	0.307	0.241
c(T)	-2.600	-2.360	-1.846	-1.368	-1.119	-1.106	-1.296	-1.630	-1.793	-1.608	-1.340
$10^*d(T)$	-0.096	-0.134	-0.211	-0.173	-0.007	0.161	0.435	0.714	0.963	1.020	0.877
e(T)	-0.238	-0.202	-0.188	-0.267	-0.341	-0.358	-0.353	-0.302	-0.235	-0.235	-0.246
$\alpha(T)$	2.310	2.144	2.030	2.209	2.523	2.610	3.804	3.356	2.729	2.487	2.606
$\beta(T)$	0.230	0.218	0.198	0.182	0.176	0.182	-0.453	-0.503	-0.540	-0.541	-0.494
N(T)	2	2	2	2	2	2	1	1	1	1	1
$\zeta = 0.05$											
b(T)	0.304	0.299	0.291	0.283	0.281	0.287	0.313	0.347	0.354	0.316	0.250
c(T)	-2.560	-2.340	-1.887	-1.471	-1.249	-1.240	-1.436	-1.757	-1.910	-1.748	-1.477
$10^*d(T)$	-0.084	-0.130	-0.211	-0.158	-0.011	0.128	0.376	0.664	0.963	1.060	0.925
e(T)	-0.257	-0.230	-0.222	-0.288	-0.352	-0.366	-0.363	-0.319	-0.262	-0.258	-0.263
$\alpha(T)$	2.410	2.256	2.150	2.309	2.602	2.670	3.869	3.423	2.779	2.494	2.559
$\beta(T)$	0.231	0.222	0.203	0.188	0.181	0.185	-0.450	-0.496	-0.530	-0.528	-0.484
N(T)	2	2	2	2	2	2	1	1	1	1	1

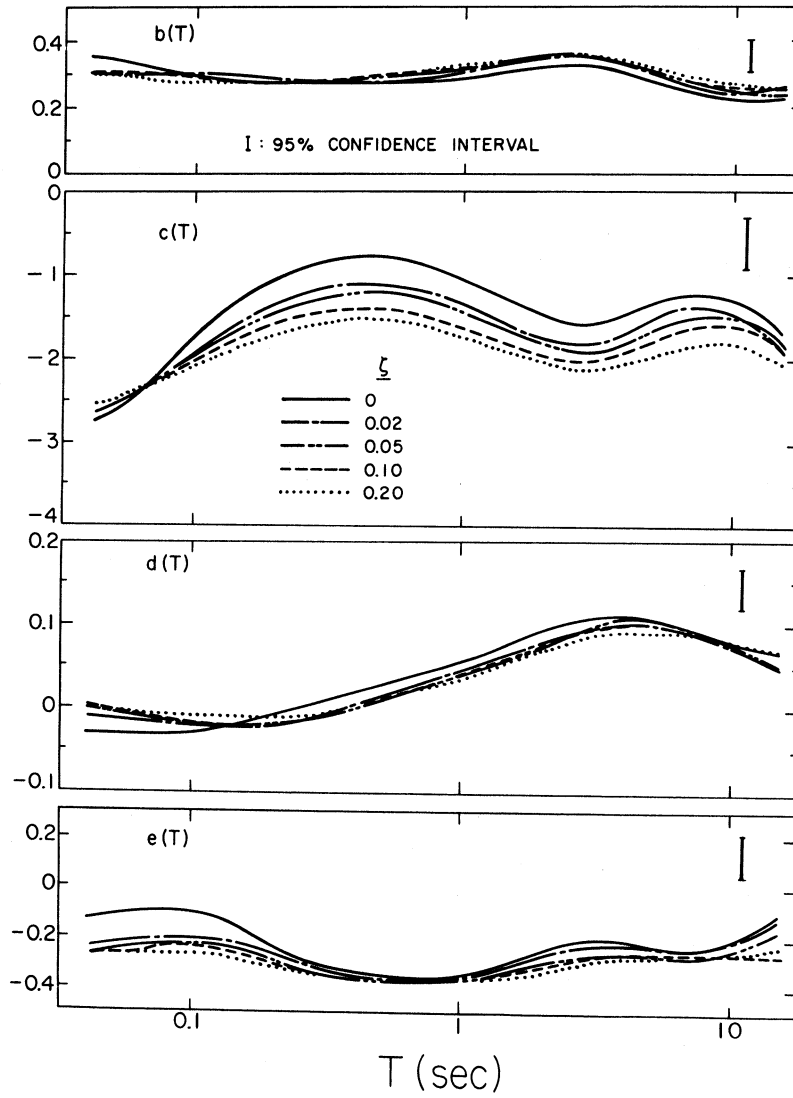


Figure 25

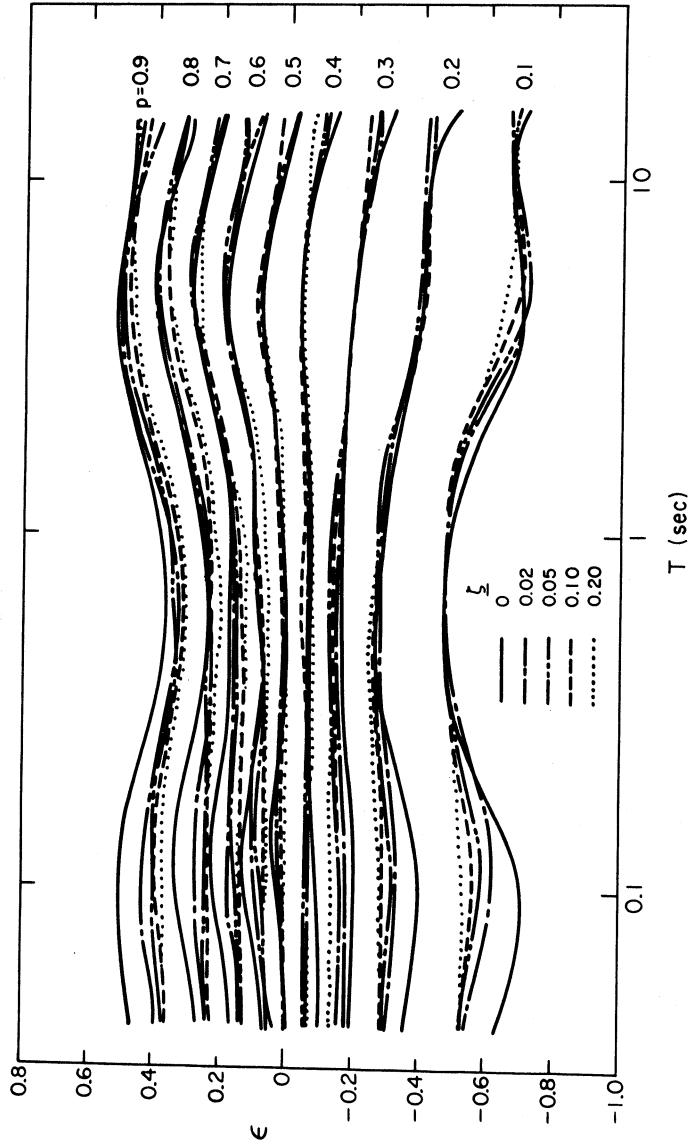


Figure 26

The coefficients $\alpha(T)$, $\beta(T)$ and $N(T)$ in equation (3), which also applies here, are also given in Table III. By choosing the probability that $\log_{10}PSV(T)$ will not be exceeded, computing the corresponding $\epsilon(T)$ and adding this to $PSV(T)$ amplitudes in equation (4) will yield a distribution of spectral amplitudes for given I_{MM} , h and v .

Figure 27 shows the plot of $\alpha(T)$, $\beta(T)$ and $N(T)$ versus T computed from regression analysis of the data on $\epsilon(T)$ (Figure 26) and in terms of the assumed distribution function given by equation (3). The expected value $\mu(T)$ and the standard deviation $\sigma(T)$ of this distribution are also shown in Figure 27. Figure 28 shows the smoothed largest differences (Kolmogorov-Smirnov test) between the distribution of $\epsilon(T)$ as modeled by equation (3) and the data (Figure 26) as well as the amplitudes of χ^2 test versus period T . Comparisons with theoretical limits corresponding to the 95% confidence level show that the distribution function, defined in equation (3), together with the scaling functions $\alpha(T)$, $\beta(T)$ and $N(T)$, is an acceptable candidate for analytic approximation of the distribution of $\log_{10}[PSV(T)]$ with respect to the estimate $\log_{10}[\hat{PSV}(T)]$.

Figures 29 through 38 present examples of $PSV(T)$ spectral amplitudes computed from equation (4) and for $MMI = IV, VI, VIII, X$ and XII , $h = 0, 4$ km, $\zeta = 0.0, 0.02, 0.05, 0.10$ and 0.20 , and for vertical and horizontal motions. The plotted amplitudes for MMI levels X and XII are outside the range where data is now available and thus cannot be tested. Those amplitudes should be considered here only as an illustration of what results from extrapolating on the basis of equation (4). Figures 39, 40 and 41 show comparison of spectra based on equation (4) ($MMI = VIII$, $h = 19,500$ ft), and the corresponding spectra from recorded accelerograms.

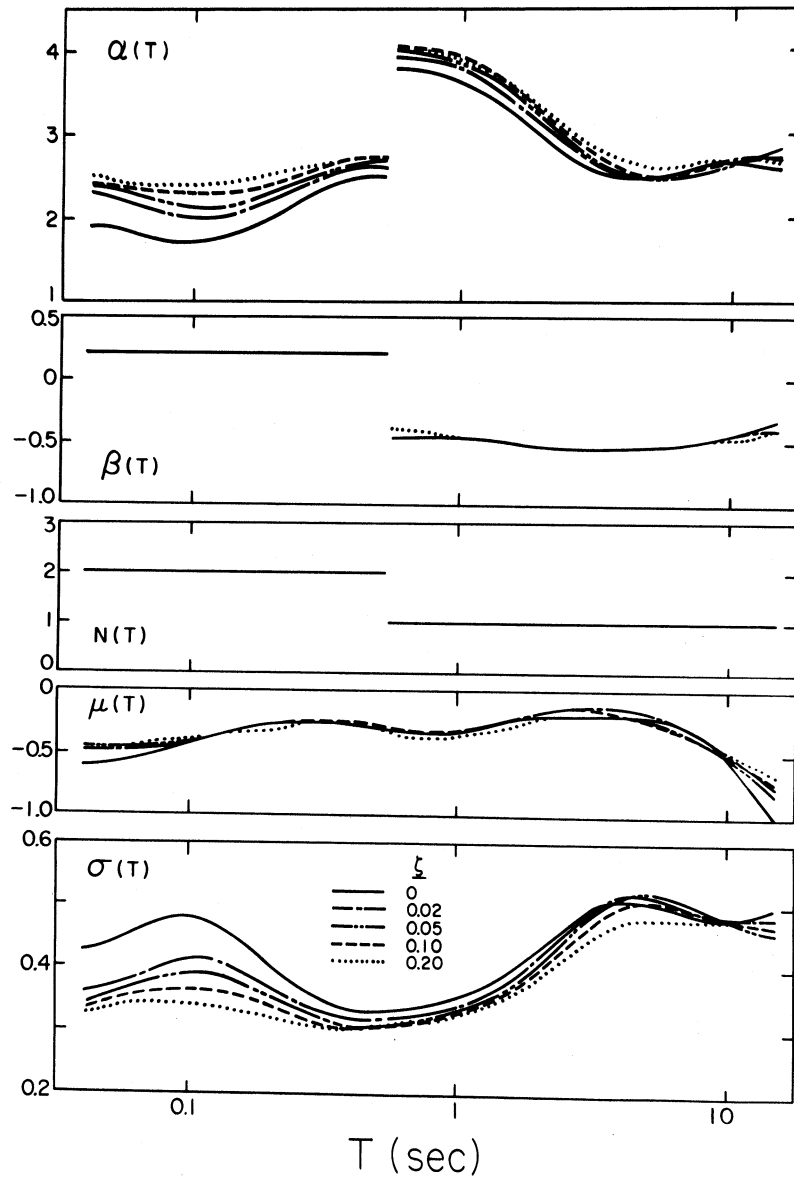


Figure 27

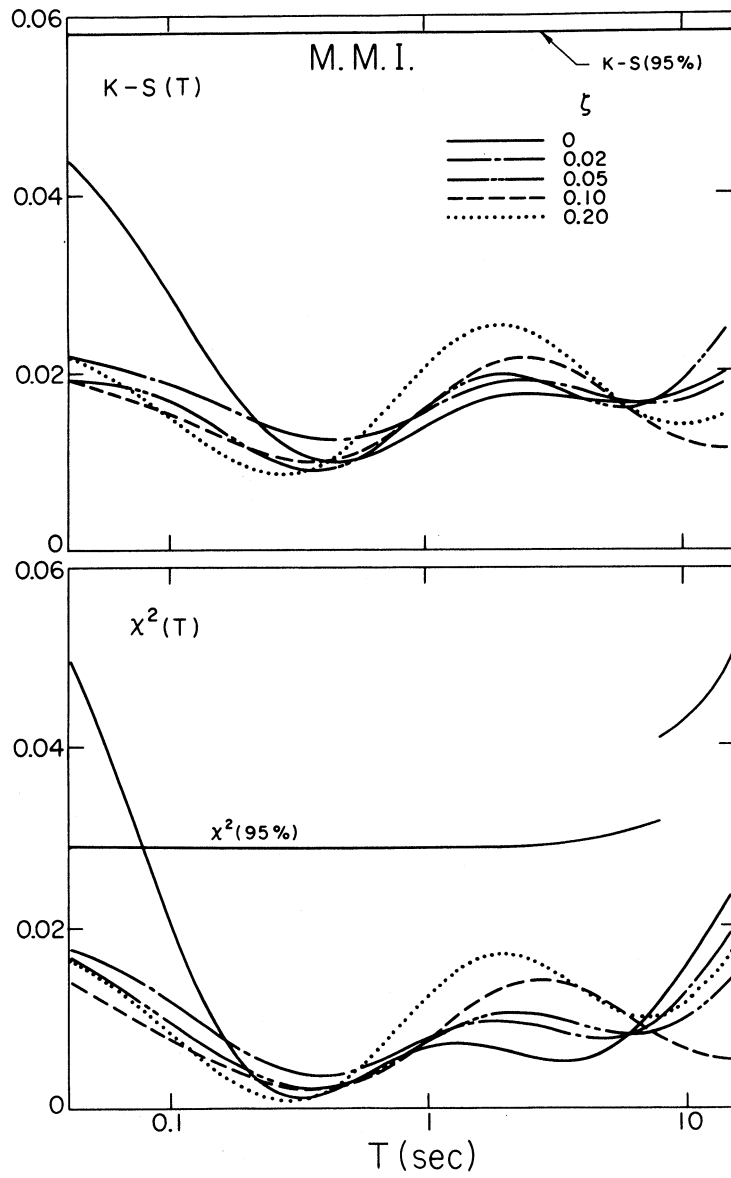


Figure 28

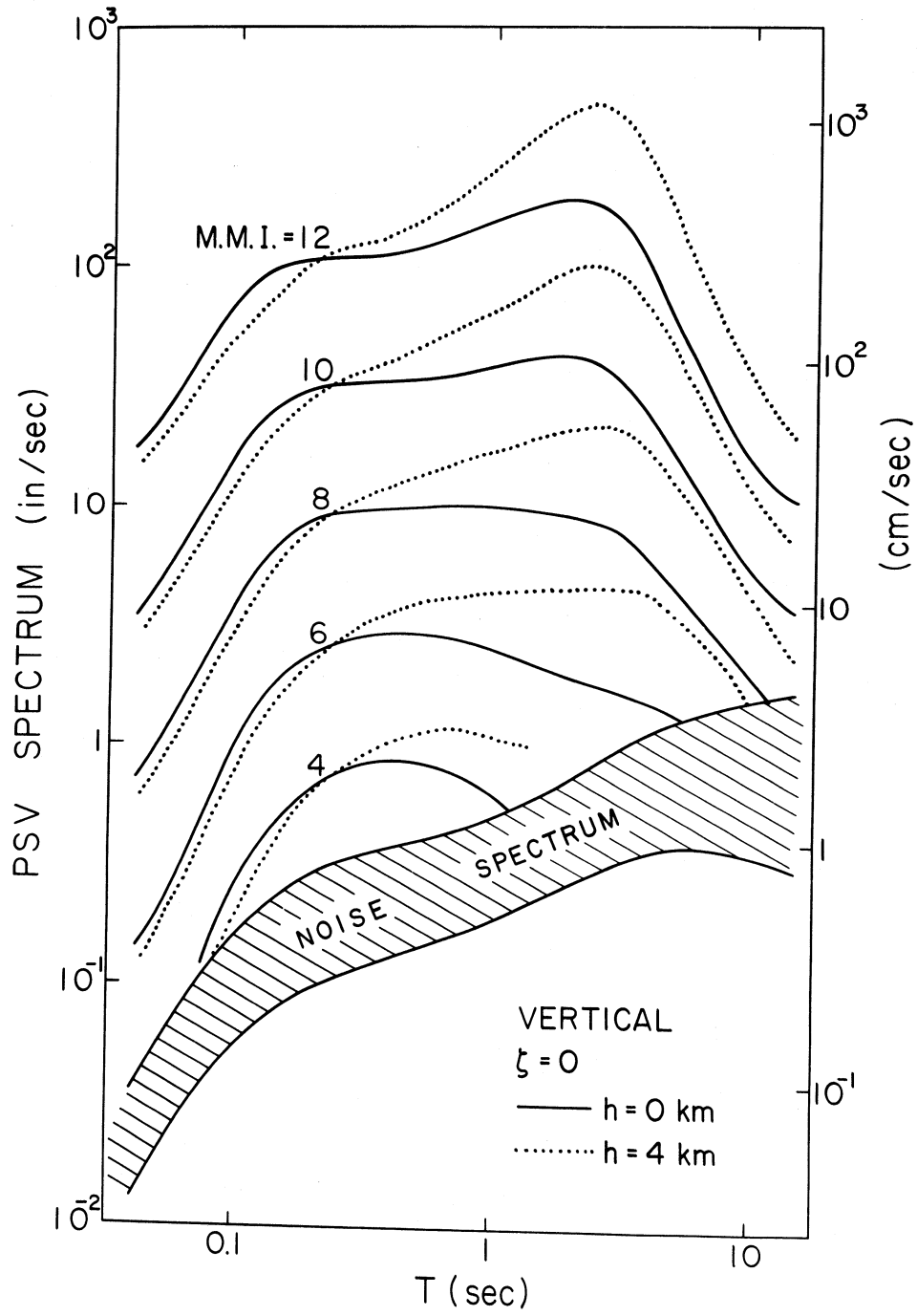


Figure 29

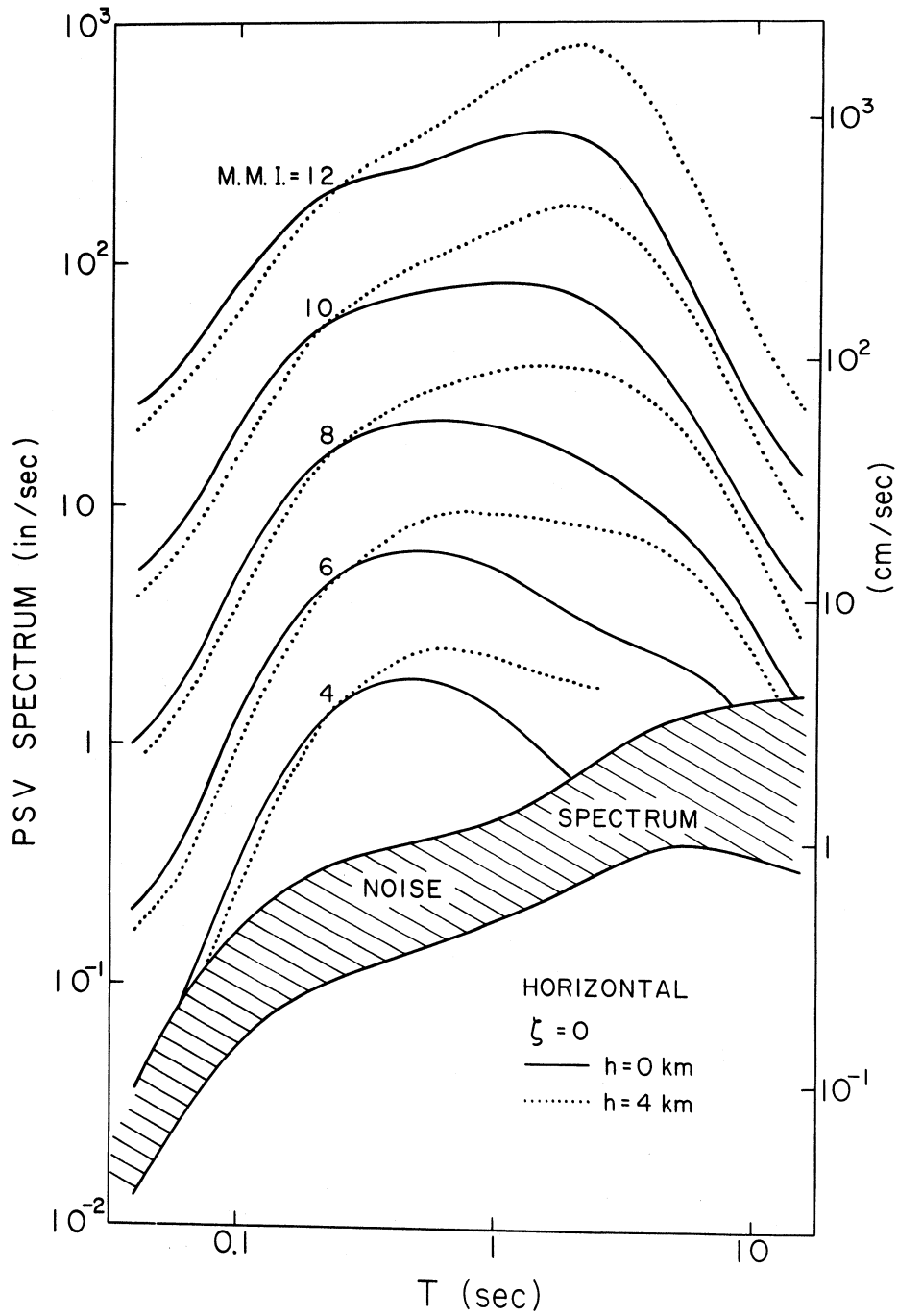


Figure 30

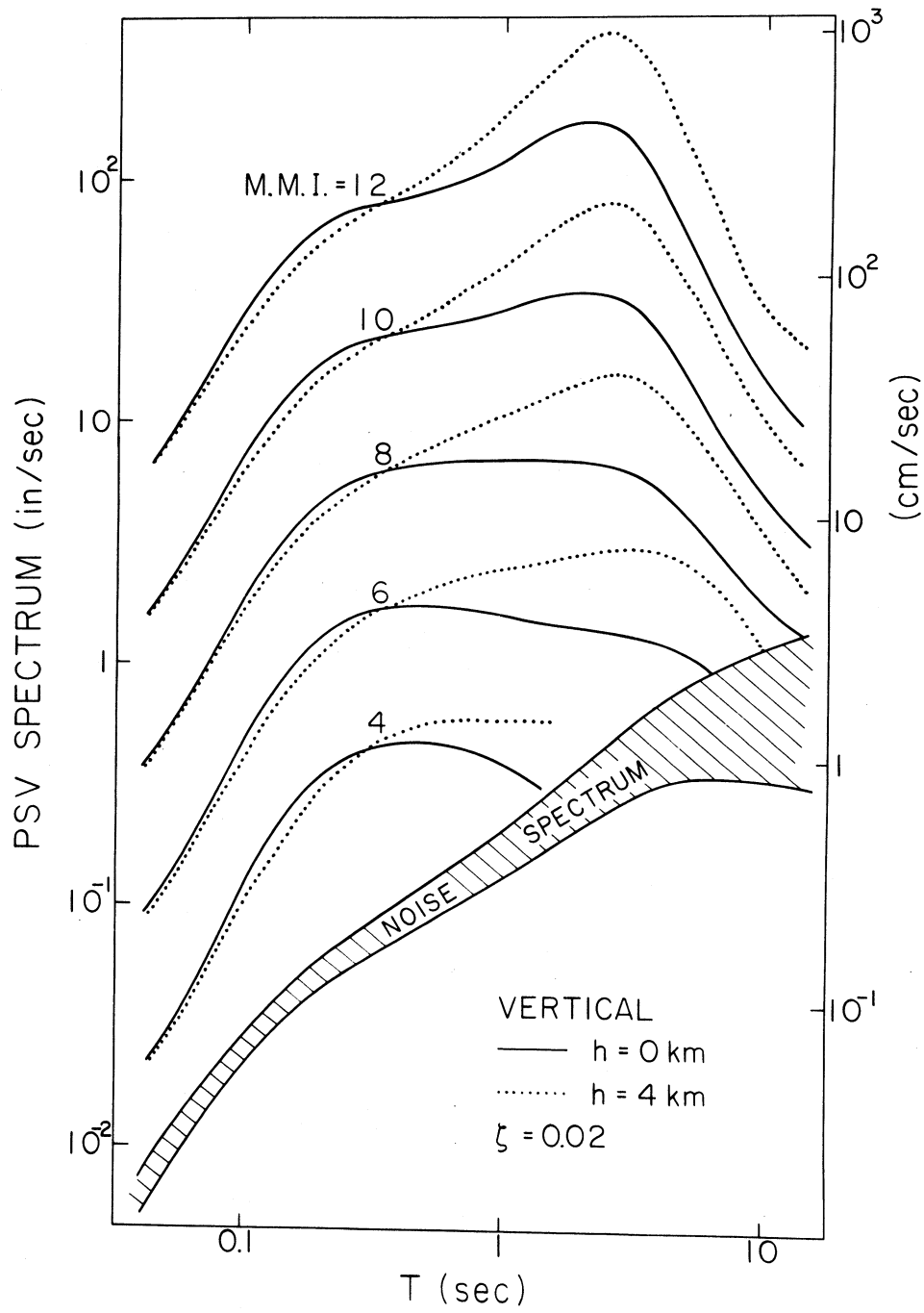


Figure 31

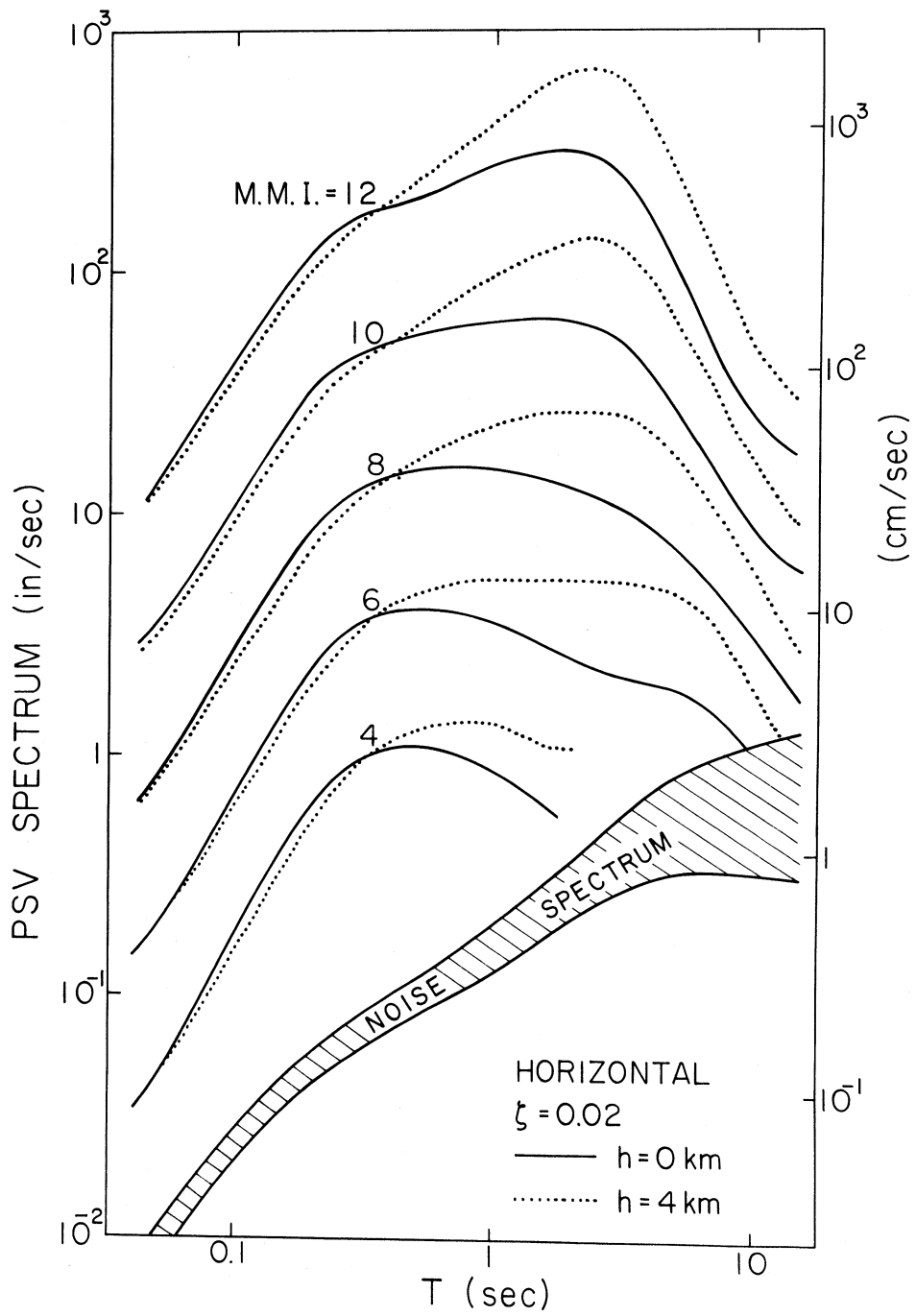


Figure 32

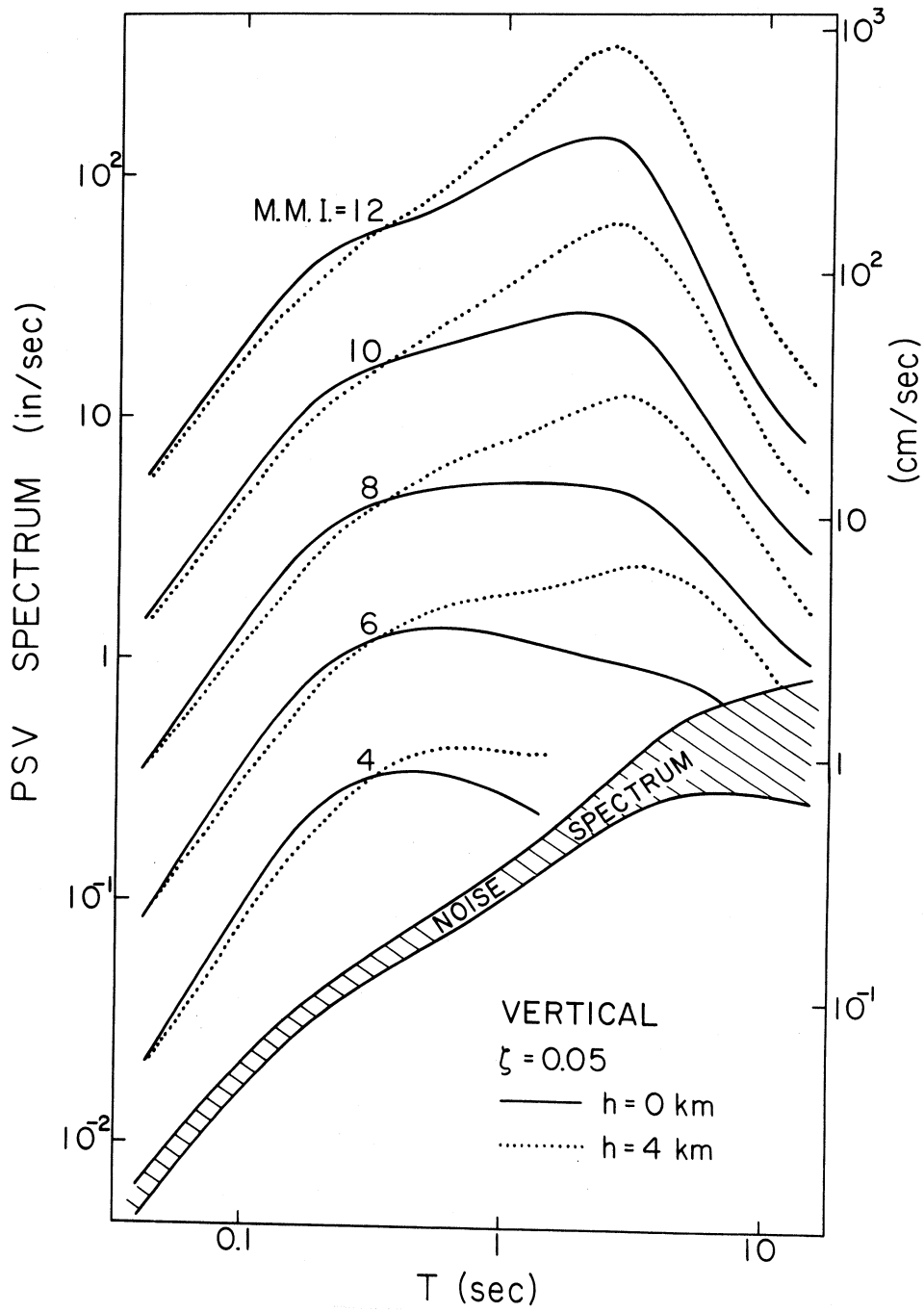


Figure 33

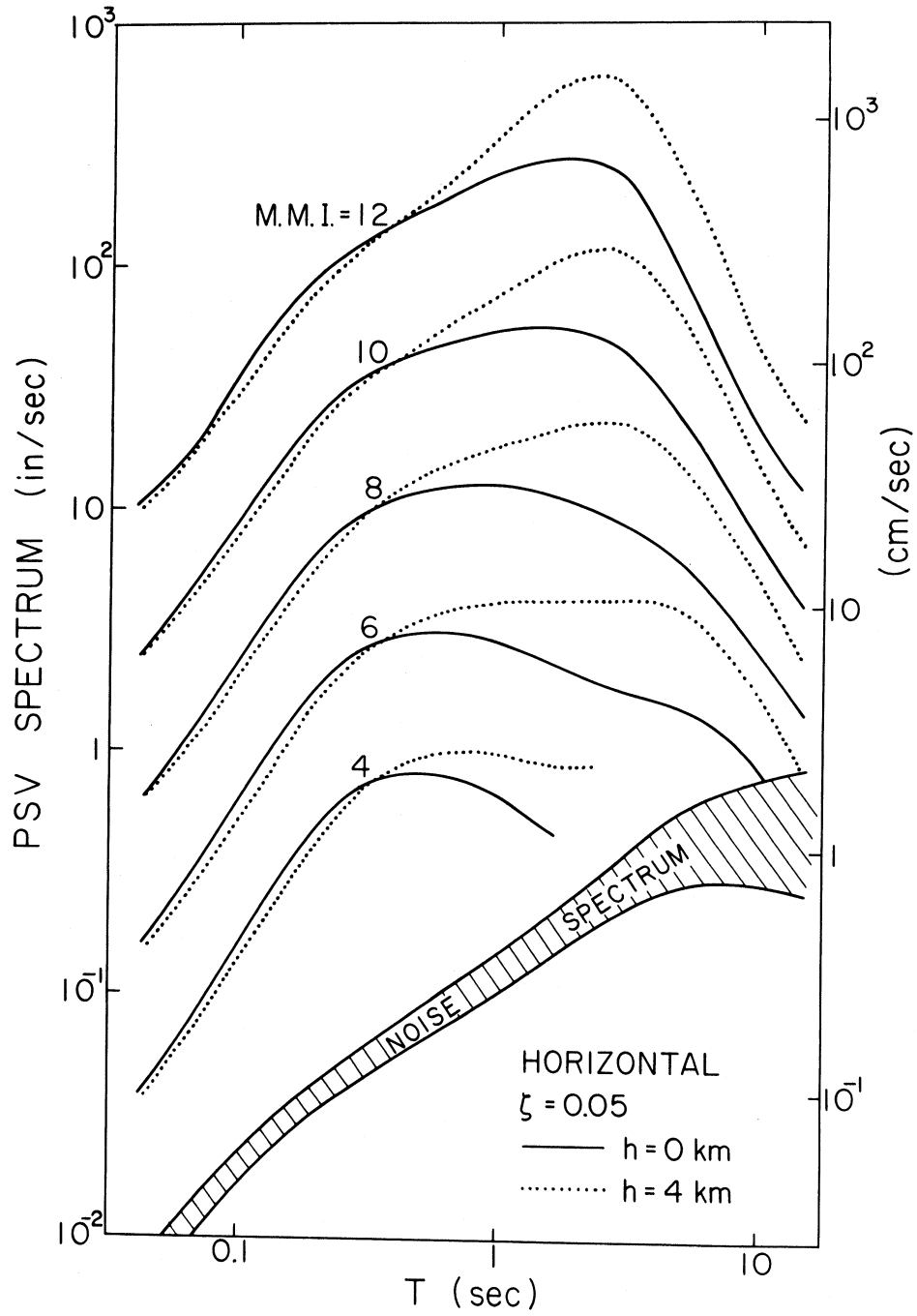


Figure 34

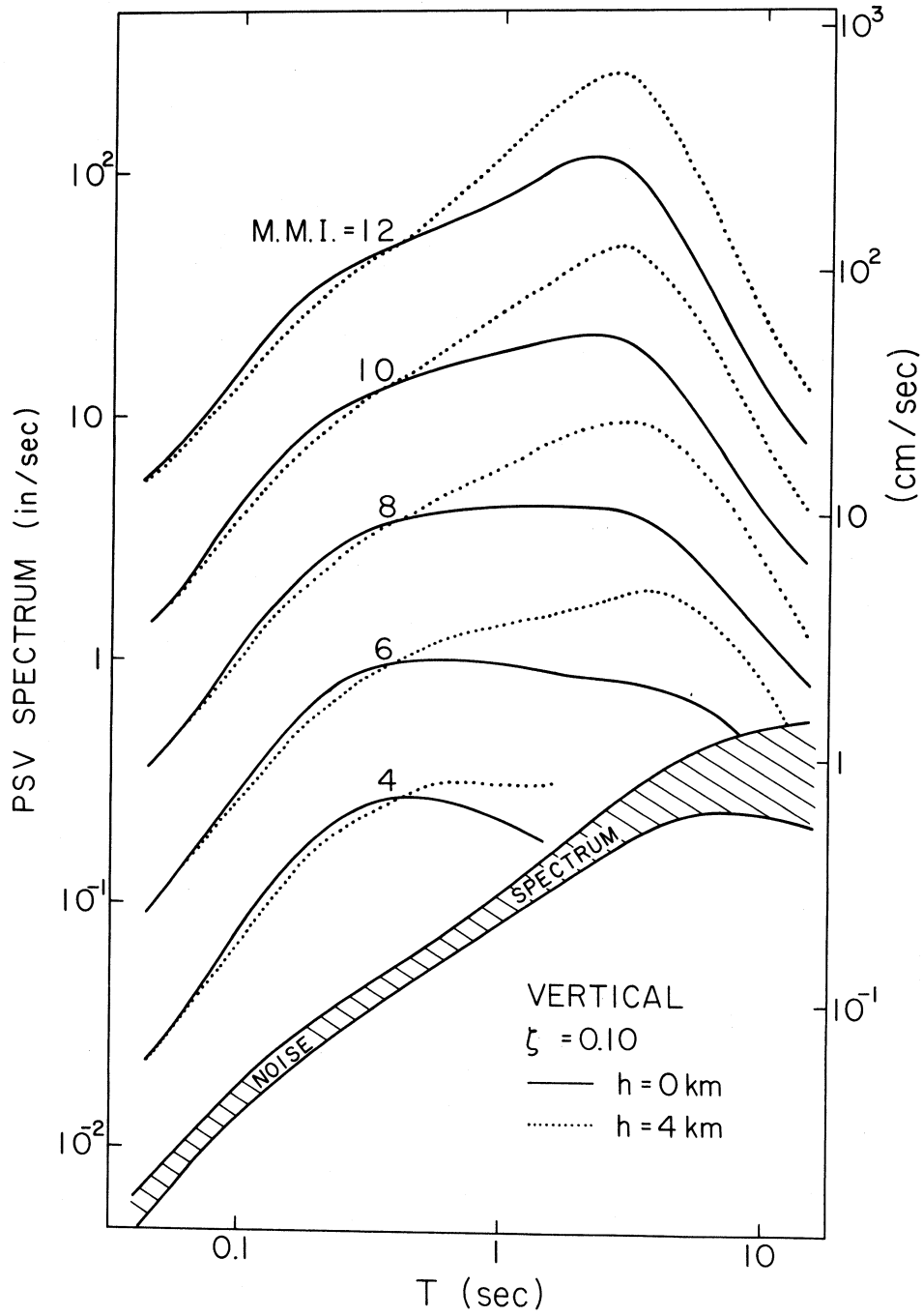


Figure 35

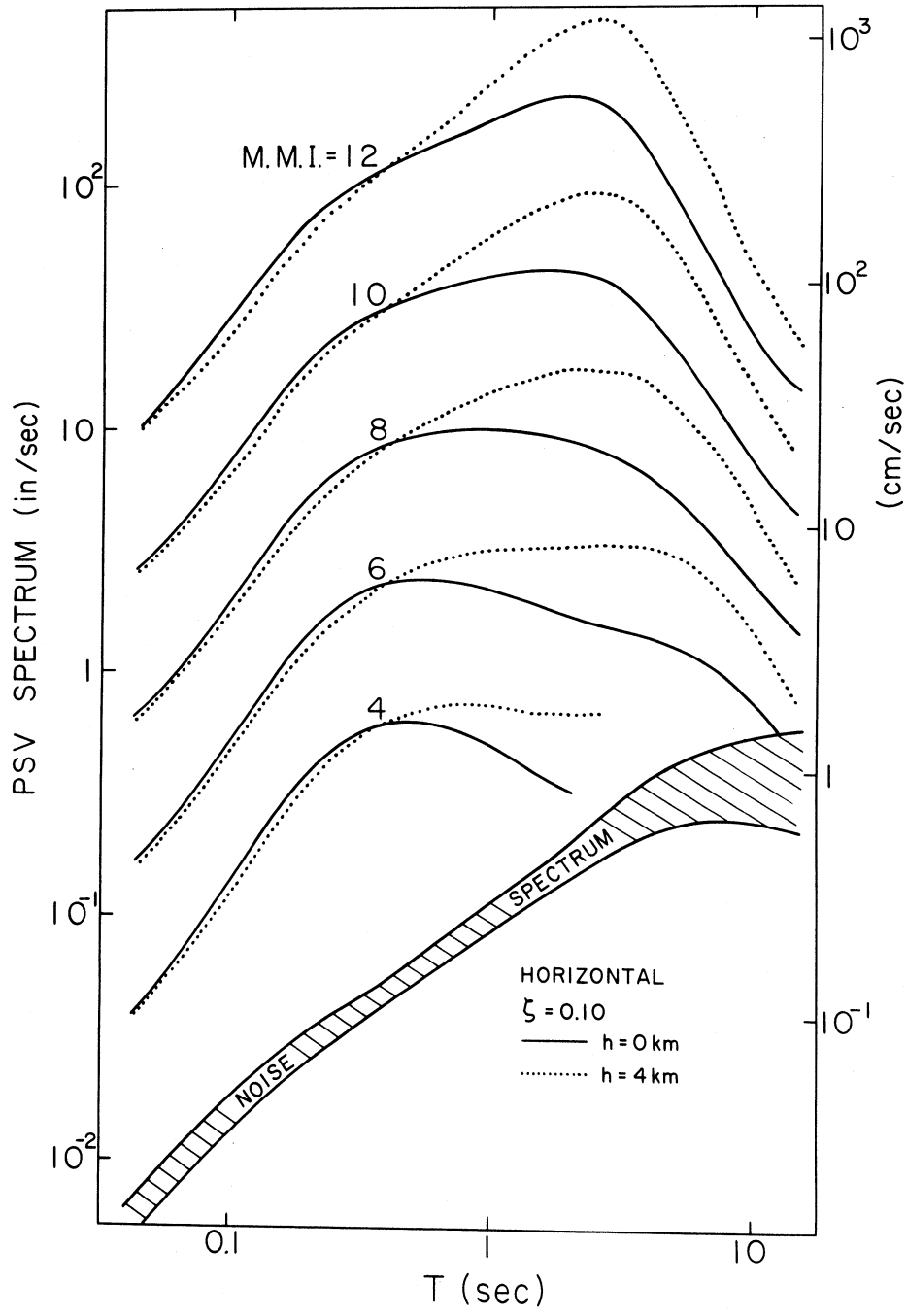


Figure 36

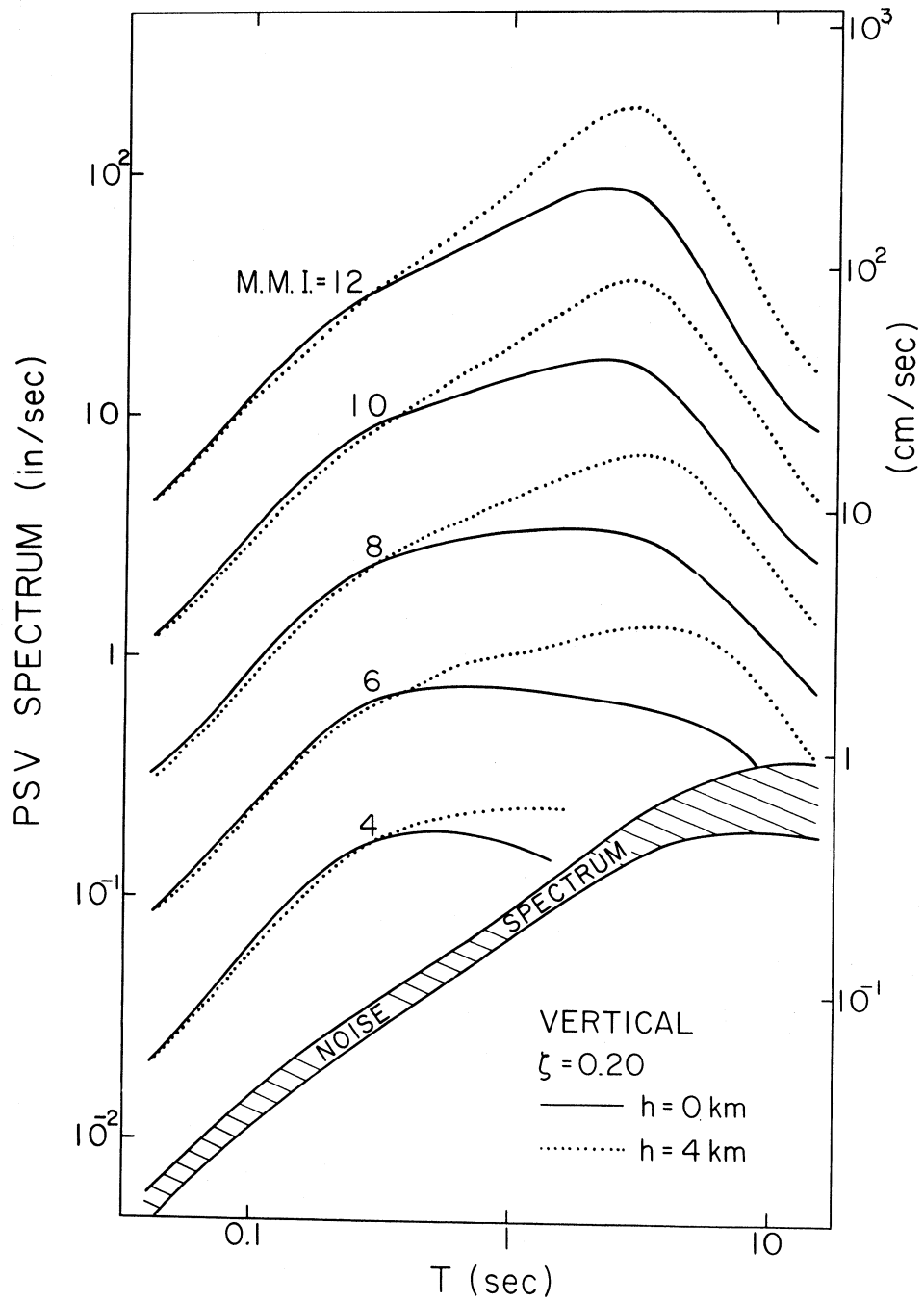


Figure 37

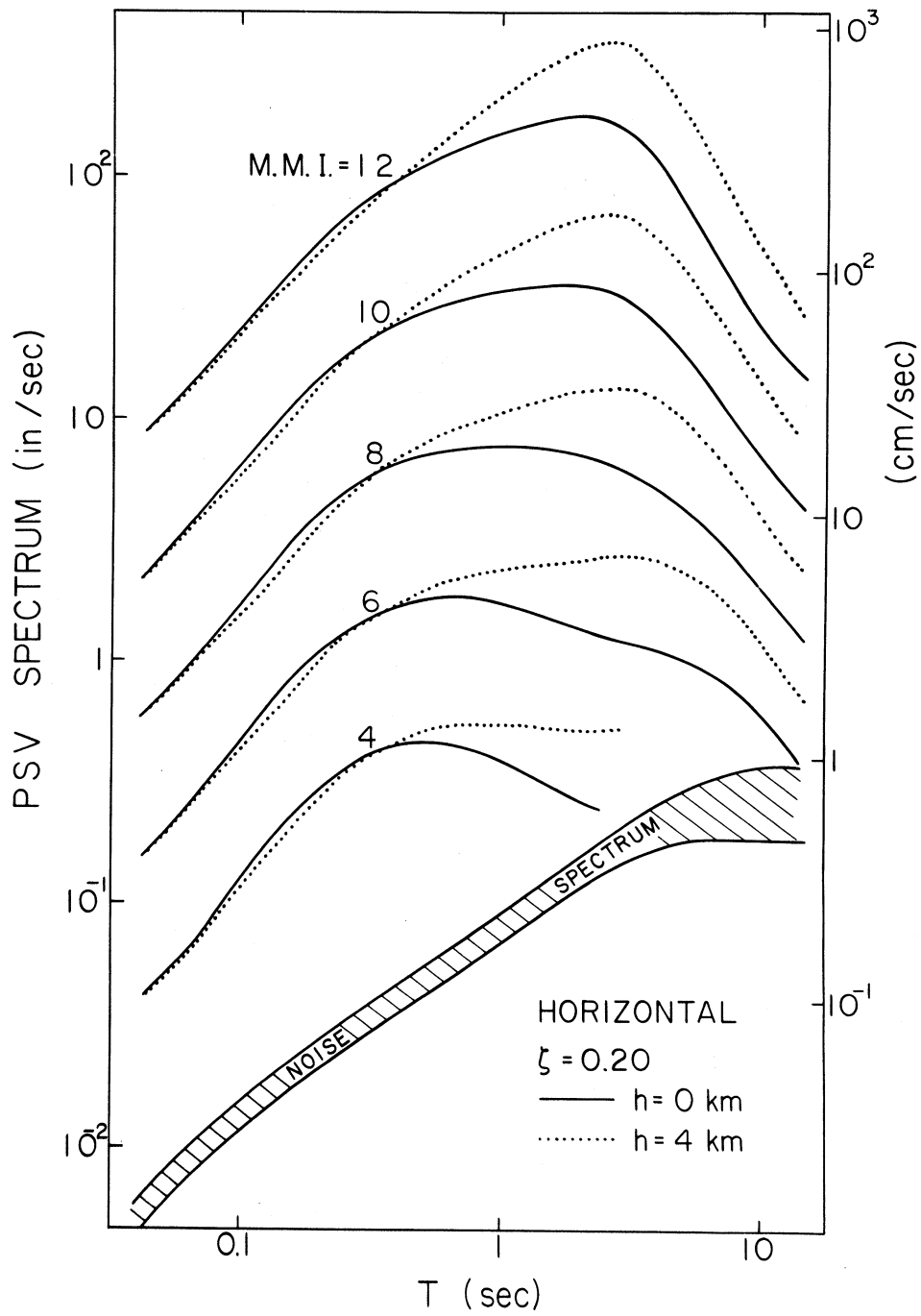


Figure 38

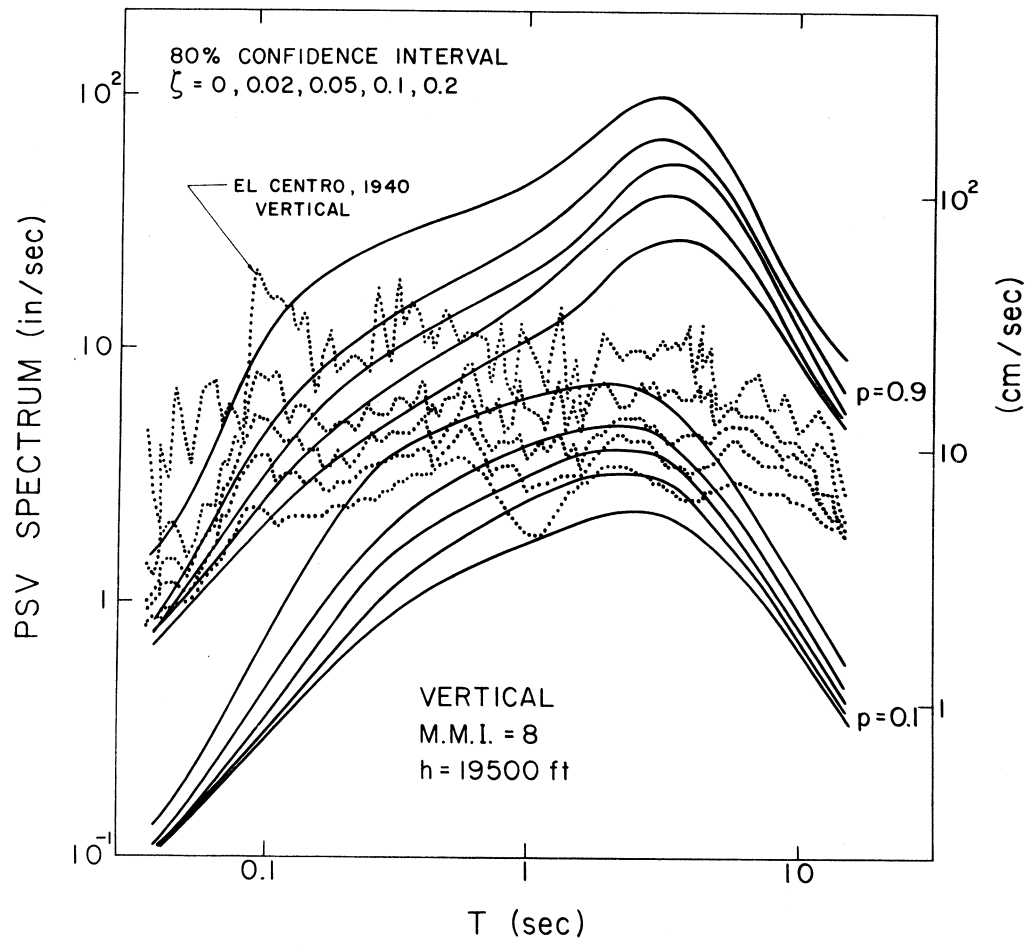


Figure 39

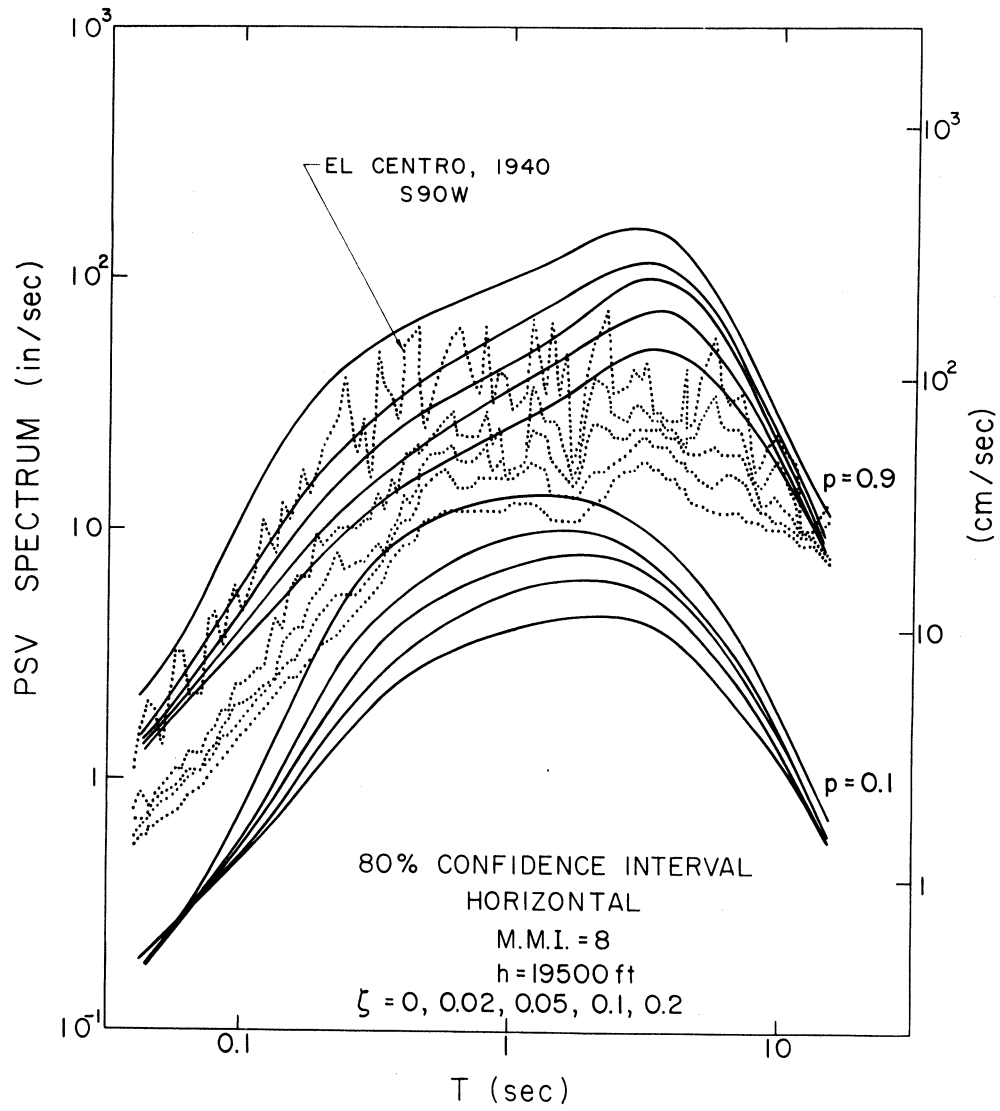


Figure 40

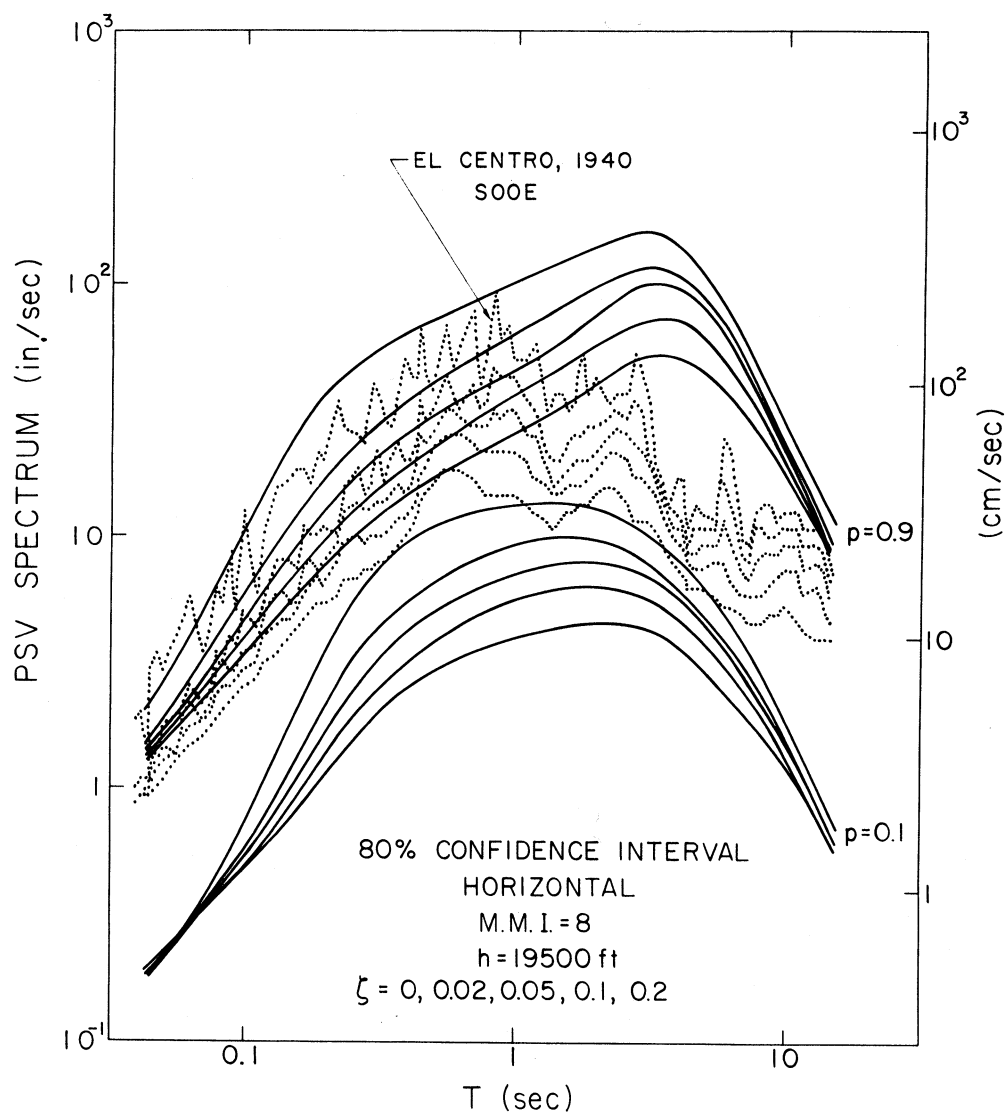


Figure 41

As suggested by Trifunac and Anderson (1977; 1978a,b) and Trifunac and Lee (1978), it is useful to check the internal consistency between equations (1) and (4). Considering the distribution of the available data among different epicentral distances, magnitudes and site intensities (Trifunac and Anderson, 1977), it is seen that the "degree of extrapolation" into the range of "largest amplitude of motion" is smaller for equation (1) than for equation (4). The bulk of the available data is now distributed between $M=4.0$ and $M=7.5$ and between $MMI = IV$ and $MMI = VII$ through $VIII$. If the "largest amplitudes of strong shaking" correspond to $M=7.5$ to 8 with $R=0$ km and $MMI = XII$, it will be seen that because of the saturation of the magnitude scale near $M=7.5$ to 8 (Trifunac, 1976; Trifunac and Anderson, 1977) equation (1) formally does not require much extrapolation before $M=M_{max}$ is reached. On the other hand, extrapolation to $MMI = XII$ on the basis of a regression model based on the data between $MMI = IV$ to $VIII$ is considerable, since there are four intensity levels between $MMI = VIII$ and $MMI = XII$ as there are between $MMI = IV$ and $MMI = VIII$. Figures 42 and 43 show the largest amplitudes of PSV spectra for $M=8.5$ and $R=0$ and for $MMI = XII$. Both sets of spectra are plotted for $h=2$ km, $\zeta=0.0, 0.02, 0.05, 0.10$ and 0.20 , and for vertical and horizontal motions. It is concluded from these figures that the slope of equation (4) with respect to I_{MM} is not contradicted by comparison with extrapolation based on equation (1).

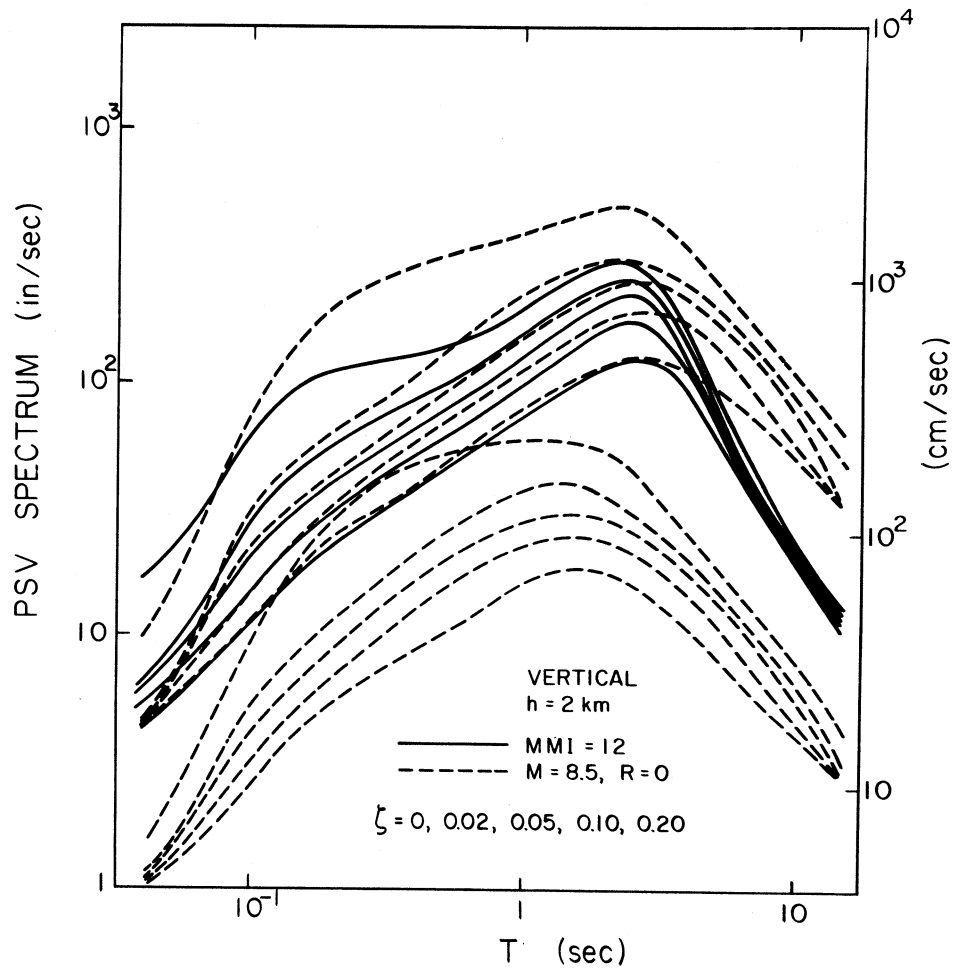


Figure 42

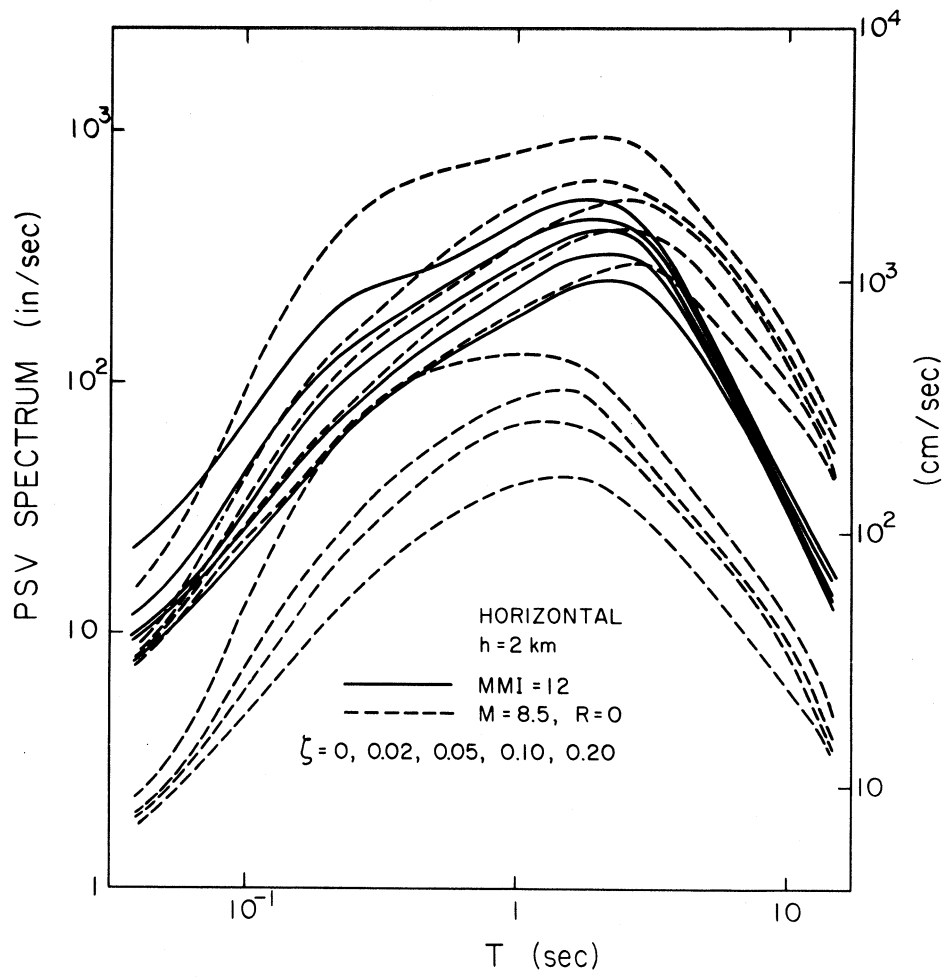


Figure 43

CONCLUSIONS

The empirical scaling equations for PSV spectrum amplitudes presented in this paper display a number of trends in the amplitudes of strong earthquake shaking which should be useful for their estimation. Inasmuch as so-far available data has been employed in this work, together with detailed scaling relationships which were tested previously in similar (Trifunac and Lee, 1978) and related analyses (Trifunac and Anderson, 1977; 1978a,b), it is noted here that the nature of these models must be considered as preliminary only. These models will have to evolve continuously through introduction of additional significant scaling parameters and through the improvement in the existing functional form of equations like (1) and (4). These improvements must be based on the physical nature of the phenomenon and various present and future new terms in the empirical scaling function should be based on the functional form predicted by theory and experiment.

Numerous recent analyses with objectives similar to those in this paper, have addressed the problem of empirical scaling of strong motion characteristics through the formalism of a regression analysis only and on the basis of often arbitrary functional forms which are convenient for the fitting routines but cannot be judged by known physical features of the problem. An attenuation often chosen in many regression analyses of the amplitudes of strong shaking is of the form $(a + R)^{-n}$, for example, where a and n are constants determined through some fitting routine. While this functional form of attenuation can model one type of wave in one distance range, it is not capable of describing the

near-field terms ($\sim R^{-4}$, $\sim R^{-2}$), body waves ($\sim R^{-1}$) and surface waves ($\sim R^{\frac{1}{2}}$) simultaneously in one scaling relation. By using $\log_{10} A_0(R)$ determined empirically in southern California, we have, through experimental means, approached the attenuation description in a physically proper way. In this sense, as many terms as possible in the empirical regression analysis should be based on, or be directly motivated by, the functional forms known to us from the earthquake fracture mechanics and the wave propagation theory. Formal regression analyses may eventually suggest the proper scaling forms but sound theoretical basis or at least consideration of the known laws of wave propagation coupled with detailed regression analysis of recorded motions will provide much faster and more direct avenues towards the improved scaling relationships. Though such principles have governed our choice of terms in equations (1) and (4), much remains to be improved. For example, it is clear that the attenuation of amplitudes with distance must depend on the size of the fault relative to R and thus, on M or MMI at the epicenter. It also must depend on the geologic features of the propagation path in the sense analogous to the effects of local geologic conditions. Inasmuch as it is possible to develop theoretical models for such dependence, the present data base seems inadequate to justify detailed analyses of this type because the small number of recordings is just not sufficient to test and discriminate among many specific theoretical assumptions.

At present, the simple rough models in equations (1) and (4) show that there is significant effect of geologic site conditions in intermediate and long period waves. The average values of response

amplitudes increase with depth, h , of local sediments, if the period of ground motion is longer than about 0.3 sec. The scatter in particular recordings with respect to these average trends, however, increases with the size and complexity of the geologic conditions. For periods shorter than about 0.3 sec amplitude changes with h are small. Though the systematic trends appear and lead to larger amplitudes on igneous basement rocks there, the data and the scaling models considered do not lead to $d(T)$ which is significantly different from zero at high frequencies.

The changes of PSV spectrum amplitudes and of its overall shape depend simultaneously on magnitude, local intensity, epicentral distance, horizontal versus vertical motions, local geologic conditions and the probability that certain amplitudes of a chosen T will be exceeded. In practical terms, this means that the common procedure(s) for prediction of response spectrum amplitudes in terms of some peak of ground motion (typically peak acceleration) and a "standard spectrum shape(s)" cannot provide a scaling method which is capable of producing spectral amplitudes which are consistent with recordings at all levels of shaking, under different local conditions and uniformly for all periods of motion. The direct method of estimating spectral amplitudes as presented here offers all these advantages simultaneously and eliminates the uncertainties which result from using the scaling in terms of peak acceleration.

REFERENCES

- Anderson, J.G. (1979). Uniform Risk Fourier Amplitude Spectra Derived from Intensity Data on Earthquake Occurrence, NUREG/CR=0689, E1-E27.
- Anderson, J.G., and M.D. Trifunac (1977). Current Computational Methods in Studies of Earthquake Source Mechanisms and Strong Ground Motion, Proc. Symp. Appl. Comp. Methods in Engr., USC, Los Angeles, Vol. II, 929-939.
- Richter, C.F. (1958). Elementary Seismology, Freeman and Co., San Francisco.
- Trifunac, M.D. (1971). Response Envelope Spectrum and Interpretation of Strong Earthquake Ground Motion, Bull. Seism. Soc. Amer., 61, 343-356.
- Trifunac, M.D. (1973). Analysis of Strong Earthquake Ground Motion for Prediction of Response Spectra, Int. J. Earthquake Eng., and Struc. Dyn., Vol. 2, 59-69.
- Trifunac, M.D., and A.G. Brady (1975). On the Correlation of Seismic Intensity Scales with the Peaks of Recorded Strong Ground Motion, Bull. Seis. Soc. Amer., 65, 139-162.
- Trifunac, M.D. (1976). Preliminary Empirical Model for Scaling Fourier Amplitude Spectra of Strong Ground Acceleration in Terms of Earthquake Magnitude, Source to Station Distance and Recording Site Conditions, Bull. Seis. Soc. Amer., 66, 1343-1373.
- Trifunac, M.D. (1979). Preliminary Empirical Model for Scaling Fourier Amplitude Spectra of Strong Motion Acceleration in Terms of Modified Mercalli Intensity and Geologic Site Conditions, Int. J. Earthquake Engr. and Struc. Dyn., 7, 63-79.
- Trifunac, M.D., and J.G. Anderson (1977). Preliminary Empirical Models for Scaling Absolute Acceleration Spectra, Dept. of Civil Engr., Report No. 77-03, Univ. of Southern Calif., Los Angeles.
- Trifunac, M.D., and J.G. Anderson (1978a). Preliminary Empirical Models for Scaling Pseudo Relative Velocity Spectra, Dept. of Civil Engr., Report No. 78-04, Univ. of Southern Calif., Los Angeles.
- Trifunac, M.D., and J.G. Anderson (1978b). Preliminary Models for Scaling Relative Velocity Spectra, Dept. of Civil Engr., Report No. 78-05, Univ. of Southern Calif., Los Angeles.

- Trifunac, M.D., and V.W. Lee (1978). Dependence of the Fourier Amplitude Spectra of Strong Motion Acceleration on the Depth of Sedimentary Deposits, Dept. of Civil Engr., Report No. 78-14, Univ. of Southern Calif., Los Angeles.
- Trifunac, M.D., and V.W. Lee (1979). Automatic Digitization and Processing of Strong Motion Accelerograms, Dept. of Civil Engr., Report No. 79-15 I, II, Univ. of Southern California, Los Angeles.
- Trifunac, M.D., and B.D. Westermo (1976). Dependence of Duration of Strong Earthquake Ground Motion on Magnitude, Epicentral Distance, Geologic Conditions at the Recording Station and Frequency of Motion, Dept. of Civil Engr., Report No. 76-02, Univ. of Southern Calif., Los Angeles.
- Trifunac, M.D., and B.D. Westermo (1977). A Note on the Correlation of Frequency Dependent Duration of Strong Ground Motion with the Modified Mercalli Intensity and the Geologic Conditions at the Recording Station, Bull. Seism. Soc. Amer., 67, 917-927.
- Westermo, B.D., and M.D. Trifunac (1978). Correlation of the Frequency Dependent Duration of Strong Earthquake Ground Motion with the Magnitude, Epicentral Distance and the Depth of Sediments at the Recording Site, Dept. of Civil Engr., Report No. 78-12, Univ. of Southern Calif., Los Angeles.
- Westermo, B.D., and M.D. Trifunac (1979). Correlations of the Frequency Dependent Duration of Strong Ground Motion with the Modified Mercalli Intensity and the Depth of Sediments at the Recording Site, Dept. of Civil Engr., Report No. 79-01, Univ. of Southern Calif., Los Angeles.